THE AMERICAN MINERALOGIST
JOURNAL OF THE MINERALOGICAL SOCIETY OF AMERICA

Vol. 26 FEBRUARY, 1941 No. 2

CRYSTALLOGRAPHIC PROCEDURES*

C. W. Wolfe, *Harvard University, Cambridge, Mass.*

During the preparation of crystallographic descriptions for the new edition of Dana's *System of Mineralogy* and also in mineral descriptions from this laboratory, certain procedures are followed. These are presented here.

MEASUREMENTS

To give a concise and accurate treatment of morphological investigations a tabulation such as that in Table 1 is used. In this table "No. Times" refers to the number of times faces of the listed form were seen, and "Qual." refers to the average quality of the reflecting signal. Rare or uncertain forms are so designated, since the investigating author can determine better than the reader the validity of a form. Uncertain forms are indicated by a question mark, letters being used only for established forms.

Table 1. Presentation of Morphological Data

Form	No. Xls.	No. Times	Size	Qual.	Measured Range ϕ ρ or Other Angles	Weighted Mean ϕ ρ or Other Angles	Calculated Values ϕ ρ or Other Angles
c 001	2	4	VL*	A*			
m 110	4	8	L	B			
w 011	4	4	M	C			
d 101	1	2	S	D			
p 111	4	12	VS	E			

* VL = Very Large
L = Large
M = Medium
S = Small
VS = Very Small

A = Excellent
B = Good
C = Fair
D = Poor
E = Bad

---

* Contribution from the Department of Mineralogy and Petrography, Harvard University, No. 234.

SYMMETRY

The preferred statement of the crystal class is that of Groth (modified by A. F. Rogers, textbook, 1937), accompanied by the complete Hermann-Mauguin symbols. Corresponding Schoenflies symbols and Dana (textbook, 1932) symmetry class numbers are listed in Table 2.

TABLE 2. SYMMETRY CLASS NOTATION

System	Groth (Modified)	Hermann-Mauguin	Schoenflies	Dana (1932)
Triclinic	1. Pedial	1	C_1	32
	2. Pinacoidal	$\bar{1}$	C_i	31
Monoclinic	3. Domatic	m	C_s	30
	4. Sphenoidal	2	C_2	29
	5. Prismatic	$\frac{2}{m}$	C_{2h}	28
Orthorhombic	6. Rhombic-pyramidal	$m\ m\ 2$	C_{2v}	26
	7. Rhombic-disphenoidal	$2\ 2\ 2$	D_2	27
	8. Rhombic-dipyramidal	$\frac{2}{m}\ \frac{2}{m}\ \frac{2}{m}$	D_{2h}	25
Tetragonal	9. Tetragonal-disphenoidal	$\bar{4}$	S_4	12
	10. Tetragonal-pyramidal	4	C_4	9
	11. Tetragonal-dipyramidal	$\frac{4}{m}$	C_{4h}	8
	12. Tetragonal-scalenohedral	$\bar{4}\ 2\ m$	D_{2d}	10
	13. Ditetragonal-pyramidal	$4\ m\ m$	C_{4v}	7
	14. Tetragonal-trapezohedral	$4\ 2\ 2$	D_4	11
	15. Ditetragonal-dipyramidal	$\frac{4}{m}\ \frac{2}{m}\ \frac{2}{m}$	D_{4h}	6
Hexagonal *P* or *R**	16. Trigonal-pyramidal	3	C_3	24
	17. Rhombohedral	$\bar{3}$	C_{3i}	22
	18. Ditrigonal-pyramidal	$3\ m$	C_{3v}	21
	19. Trigonal-trapezohedral	$3\ 2$	D_3	23
	20. Hexagonal-scalenohedral	$\bar{3}\ \frac{2}{m}$	D_{3d}	20

---

* In the hexagonal system the lattice mode in classes 16–20 may be either primitive hexagonal (*P*) or rhombohedral (*R*); in classes 21–27 only the primitive mode is possible.

TABLE 2. *Continued*

System	Groth (Modified)	Hermann-Mauguin	Schoenflies	Dana (1932)
Hexagonal P*	21. Trigonal-dipyramidal	$\bar{6}$	C_{3h}	19
	22. Hexagonal-pyramidal	6	C_6	16
	23. Hexagonal-dipyramidal	$\frac{6}{m}$	C_{6h}	15
	24. Ditrigonal-dipyramidal	$\bar{6}\ m\ 2$	D_{3h}	18
	25. Dihexagonal-pyramidal	$6\ m\ m$	C_{6v}	14
	26. Hexagonal trapezohedral	$6\ 2\ 2$	D_6	17
	27. Dihexagonal-dipyramidal	$\frac{6}{m}\ \frac{2}{m}\ \frac{2}{m}$	D_{6h}	13
Isometric	28. Tetartoidal	$2\ 3$	T	5
	29. Diploidal	$\frac{2}{m}\ \bar{3}$	T_h	2
	30. Hextetrahedral	$\bar{4}\ 3\ m$	T_d	3
	31. Gyroidal	$4\ 3\ 2$	O	4
	32. Hexoctahedral	$\frac{4}{m}\ \bar{3}\ \frac{2}{m}$	O_h	1

ELEMENTS

The elements, in general, include the direct (linear) and reciprocal (polar) axial ratios and interaxial angles plus the gnomonic projection constants (when these differ from the polar values). The elements are given relative to a chosen orientation of axes and unit parametral plane. *Orientation* refers here to the relative position of the axes of a unique elementary parallelopiped. The unit morphological cell is generally chosen to conform to the structural cell when this is known. Otherwise, the unit is chosen after a consideration of various rules such as Ungemach's rule of *total of indices*, the *law of Bravais*, the generalized law of Bravais proposed by Donnay and Harker, or, preferably, Donnay's morphological method of analysis used in conjunction with Peacock's *harmonic-arithmetic rule.* A consideration of these rules usually leads to a morphological unit which conforms with that derived by x-ray study. Exceptional treatments, however, are sometimes desirable when interrelation between species can be made clearer by an unconventional treatment. Rarely, the x-ray unit involves a complication of the morphological discussion. In such cases it is not retained.

TABULATION OF FORMS AND ANGLES

The table of forms and angles following the elements should include all of the common and less common forms, with letters and important angles for each. Four categories of forms are recognized in the new edition of the Dana *System;* they are: common, less common, rare, and uncertain. These are qualitative terms referring to the occurrence in each mineral species.

Few general rules for the order of form listing can be given for all crystal systems, since each possesses restrictive peculiarities. The general order is: first, forms cutting but one crystal axis; second, those cutting two axes; third, those cutting three axes. In the hexagonal system, with four axes, a similar order is employed.

Tabulations will be found in the following pages for each crystal system, giving the order in which all possible forms in each symmetry class are listed. Complementary (or correlative) forms are grouped with their holohedral equivalents and are listed in the same order as though holohedral. In case the vertical axis is polar, the headings "lower" and "upper" are used beneath the Hermann-Mauguin symmetry class symbol. Only "upper" form indices are given, and an x in the "lower" column indicates that the form may occur as a "lower" one. In specific tabulations of the forms of such crystals the same letter is given for the "lower" as for the "upper" form, but a minus sign is placed over it ($\bar{c}$ for example). If the form is observed only as a "lower" one, its letter appears only in that column, but the indices are always those of the upper merohedral equivalent. Plus or minus signs before a form letter indicate the sign of phi of the form. Prime marks (′) to the right or left of a form letter indicate whether the form occurs to the right or left of some defined meridian. The general order for plus and minus, right and left forms is: plus right (+′), plus left (′+), minus left (′−), minus right (−′).

The angles given in the table for the representative face of each form include the azimuth phi (ϕ) and polar distance rho (ρ), angular coordinates, as well as interfacial angles to two or more fundamental faces. The angles given and their meanings will be shown in figures included in the discussion of each system.

TRANSFORMATION FORMULAE

In the transformation of elements and indices from one set to another (old to new) the transformation matrix is written in the linear form (Barker, 1930): $u_1v_1w_1/u_2v_2w_2/u_3v_3w_3$, where $(u_1u_2u_3)$,* $(v_1v_2v_3)$, and

---

* The usage of brackets followed here is:

( ) = face symbol

{ } = form symbol

[ ] = zone or axis symbol

$(w_1w_2w_3)$ are the indices, multiple if need be, in the new orientation of the old axial planes (100), (010), and (001), respectively; and where $[u_1v_1w_1]$, $[u_2v_2w_2]$, and $[u_3v_3w_3]$ in the old orientation represent the new axial lengths [100], [010], and [001], respectively.

To obtain such a formula, then, it is necessary to determine the new indices of the old axial planes (100), (010), and (001) and to write them in that order in vertical columns as shown below. It is further necessary to determine the new indices of any general face (*hkl*) or of a pair of special faces of (*hk*0), (0*kl*), and (*h*0*l*). This requirement arises from the fact that it is impossible to determine from a projection whether the new indices of the old axial planes are correct or are but the simplest expression of the actual multiple indices of the plane, as is demonstrated later. Any face symbol (*hkl*) in the old orientation may be transformed to the new equivalent $(h'k'l')$ by the formula $u_1v_1w_1/u_2v_2w_2/u_3v_3w_3$ as follows:

$$h' = u_1h + v_1k + w_1l;\quad k' = u_2h + v_2k + w_2l;\quad l' = u_3h + v_3k + w_3l.$$

The following example will serve to indicate the procedure followed to obtain a transformation formula.

Old Orientation New Orientation . . . . (1)
(100) = $(\bar{1}01) = (u_1u_2u_3)$
(010) = $(0\bar{1}0) = (v_1v_2v_3)$
(001) = $(011) = (w_1w_2w_3)$
(121) = $(\bar{1}03)$

Writing the given relations in the linear form $u_1v_1w_1/u_2v_2w_2/u_3v_3w_3$, we obtain $\bar{1}00/0\bar{1}1/101$. This formula must be checked by transforming (121) to obtain the new symbol. This is done graphically below:

$$\begin{array}{ccc} 1\ \ 2\ \ 1 & 1\ \ 2\ \ 1 & 1\ \ 2\ \ 1 \\ \times\ \times\ \times & \times\ \times\ \times & \times\ \times\ \times \\ \bar{1}\ \ 0\ \ 0\ / & 0\ \ \bar{1}\ \ 1\ / & 1\ \ 0\ \ 1 \\ \hline \bar{1}+0+0 & 0+\bar{2}+1 & 1+0+1 \\ =\bar{1} & =\bar{1} & =2 \end{array} \quad \ldots\ldots\ldots\ldots\ldots\ldots(2)$$

The new indices obtained are $(\bar{1}\bar{1}2)$ instead of the correct $(\bar{1}03)$, showing the need of adjusting the terms of the formula. By a simple cut-and-try process various multiple indices are substituted in the second column of (1). When (011) of (1) is changed to (022), the other equivalences remaining unchanged, the correct formula results.

Old New
(100) = $(\bar{1}01)$
(010) = $(0\bar{1}0)$ or $\bar{1}00/0\bar{1}2/102$ . . . . (3)
(001) = (022)

Transforming (121) as in (2) we now obtain $(\bar{1}03)$ which validates formula (3).

As was indicated earlier, this type of formula not only facilitates the transformation of indices, but it also permits the determination of the new axial directions, lengths, and angles from their identity in the old lattice. $[u_1v_1w_1]$ $[u_2v_2w_2]$, and $[u_3v_3w_3]$ in the old lattice orientation are the new [100], [010], and [001], respectively. Thus, in the transformation example just given we see that:†

$$\begin{array}{ll} \text{Old Orientation} & \text{New Orientation} \\ [u_1v_1w_1]=[\bar{1}00] & \equiv[100] \\ [u_2v_2w_2]=[0\bar{1}2] & \equiv[010] \\ [u_3v_3w_3]=[102] & \equiv[001] \end{array} \quad \text{.......... (4)}$$

Conventionally, the new interaxial angles are defined as follows:

$$\begin{array}{ll} \quad\text{New} & \text{Old} \\ \alpha'=[010]\wedge[001] & \equiv[0\bar{1}2]\wedge[102] \\ \beta'=[001]\wedge[100] & \equiv[102]\wedge[\bar{1}00] \\ \gamma'=[100]\wedge[010] & \equiv[\bar{1}00]\wedge[0\bar{1}2] \end{array}$$

The length, T, of any $[uvw]$, in this case of $[\bar{1}00]$, $[0\bar{1}2]$, or $[102]$ in the old lattice, is calculated as follows:

$$T^2_{uvw}=a^2u^2+b^2v^2+c^2w^2+2bc\cos\alpha+2ca\cos\beta+2ab\cos\gamma \text{ .... (5)}$$

(a, b, c, α, β, γ are the linear elements of the old lattice). If τ is the angle between the directions $[u_1v_1w_1]$ and $[u_2v_2w_2]$ in the old lattice, the new axial angles are computed by the general formula:

$$\cos\tau=[a^2u_1u_2+b^2v_1v_2+c^2w_1w_2+bc(v_1w_2+w_1v_2)\cos\alpha$$
$$+ca(w_1u_2+u_1w_2)\cos\beta+ab(u_1v_2+v_1u_2)\cos\gamma]/T_{u_1v_1w_1}\cdot T_{u_2v_2w_2} \text{ .... (6)}$$

For a more extended discussion of transformations see the following works:

Lewis, W. J., 1899—Crystallography, 104.
Barker, T. V., 1930—Systematic Crystallography, 32–34.
Donnay, J. D. H., 1937—*Am. Mineral.*, **22**, 621–624.
Peacock, M. A., 1937—*Am. Mineral.*, **22**, 588–620.
Richmond, W. E., 1937—*Am. Mineral.*, **22**, 630–642.
Wolfe, C. W., 1937—*Am. Mineral.*, **22**, 736–741.
International Tables, 1935—**1**, 73–76.

THE TRICLINIC SYSTEM

Elements. The elements in the triclinic system include: the linear axial ratio $a:b:c$ $(b=1)$ and interaxial angles α, β, γ; the polar axial ratio $p_0:q_0:r_0$ $(r_0=1)$ and interaxial angles λ, μ, ν; and the gnomonic projection constants p_0', q_0', x_0', y_0'. In the triclinic system the gnomonic projection values are greater than the polar values, since r_0 of the polar ratio, which is taken as unity and normal to c (001), is inclined to the center of the projection.

---

† The sign ≡ is read "equals after transformation."

The plane of projection of the polar elements thus drops an amount which is a function of the rho value of *c* (001). The gnomonic projection plane $A'B'C'D'$ (Fig. 1) drops to the position $ABCD$ of the polar elements, both parallel to the equatorial plane. The position of $ABCD$ is determined by the point of emergence on the sphere of projection of the normal to *c* (001).

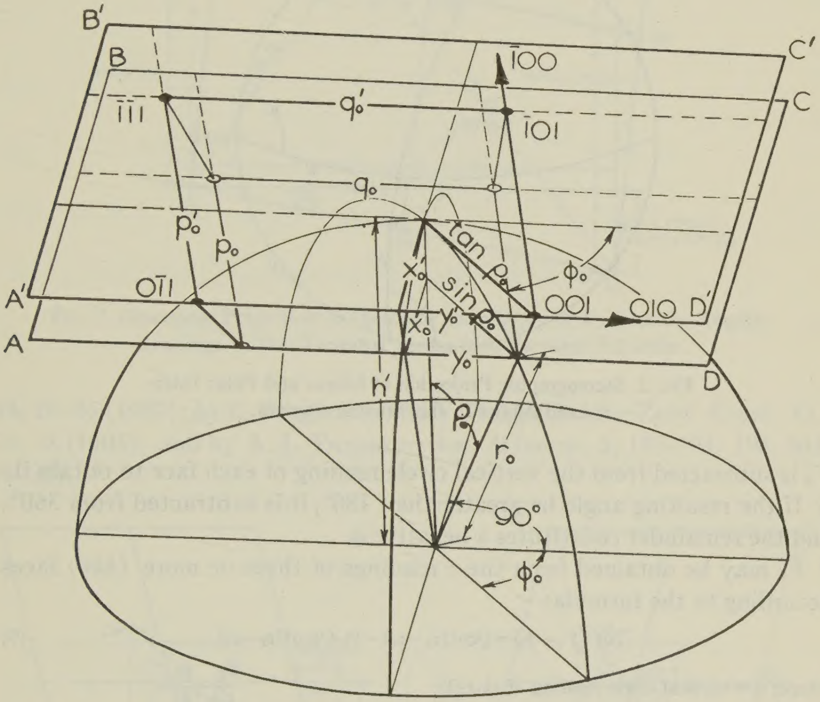

FIG. 1. Relation of Gnomonic Projection Elements to Polar Elements in the Triclinic System.

The linear interaxial angles α, β, γ are defined as follows:

$$\alpha=[010]\wedge[001],\ \beta=[001]\wedge[100],\ \gamma=[100]\wedge[010] \ldots\ldots\ldots\ldots\ldots (7)$$

The polar axial angles λ, μ, ν are the following interfacial angles:

$$\lambda=(010)\wedge(001),\ \mu=(001)\wedge(100),\ \nu=(100)\wedge(010) \ldots\ldots\ldots\ldots\ldots (8)$$

The six angles are shown in stereographic projection (Fig. 2).

The projection constants used in calculations are shown in Figs. 4*a* and 4*b*, which differ only in the obliquity of ν.

Calculation of V_0. The first step in the determination of the elements from two-circle goniometrical measurements is the calculation of V_0, the best average vertical circle goniometer reading for the normal to (010), which is chosen as the zero meridian. When b (010) is well developed and reflects well, its v reading may be made V_0. The best value for

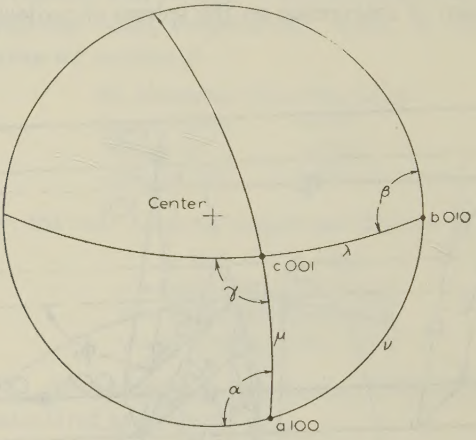

Fig. 2. Stereographic Projection of Linear and Polar Interaxial Angles in the Triclinic System.

V_0 is subtracted from the vertical circle reading of each face to obtain its ϕ. If the resulting angle be greater than 180°, it is subtracted from 360°, and the remainder constitutes a negative ϕ.

V_0 may be obtained from the v readings of three or more $(hk0)$ faces according to the formula:

$$\cot(V_0 - v_2) = Q\cot(v_3 - v_1) - (1\text{-}Q)\cot(v_2 - v_1) \quad \ldots\ldots (9)$$

where: v_1 = vertical circle reading of (h_1k_10);
v_2 = vertical circle reading of (h_2k_20);
v_3 = vertical circle reading of (h_3k_30);

$$Q = \frac{\dfrac{k_3}{h_3} - \dfrac{k_2}{h_2}}{\dfrac{k_3}{h_3} - \dfrac{k_1}{h_1}}$$

V_0 is also calculated from measurements of various pairs of terminal faces, each pair having the same h/l value, according to the following formula:

$$\text{Tan } V_0 = \frac{(\sin v_2 \tan \rho_2) - (\sin v_1 \tan \rho_1)}{(\cos v_2 \tan \rho_2) - (\cos v_1 \tan \rho_1)} \quad \ldots\ldots (10)$$

where v_1, ρ_1; v_2, ρ_2 are the angular readings of the two faces (Fig. 3). This calculation is repeated for several pairs of such faces, and the results averaged. Due attention must be given to the signs of the trigonometric functions.

Extended demonstrations and illustrations of the use of (9) and (10) are given by C. Dreyer and V. Goldschmidt—*Meddelelser om Grønland*, **34,** 29–36 (1907); by L. Borgstrom and V. Goldschmidt—*Zeits. Kryst.*, **41,** 75–78 (1905); and by A. L. Parsons—*Am. Mineral.*, **5,** 193-194, 198–203 (1920).

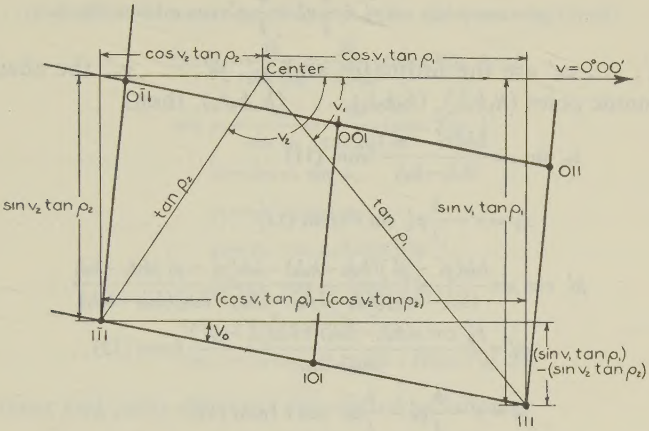

FIG. 3. Gnomonic Projection to Illustrate Calculation of V_0 from the Angular Readings of Two Terminal Forms with the same h/l value.

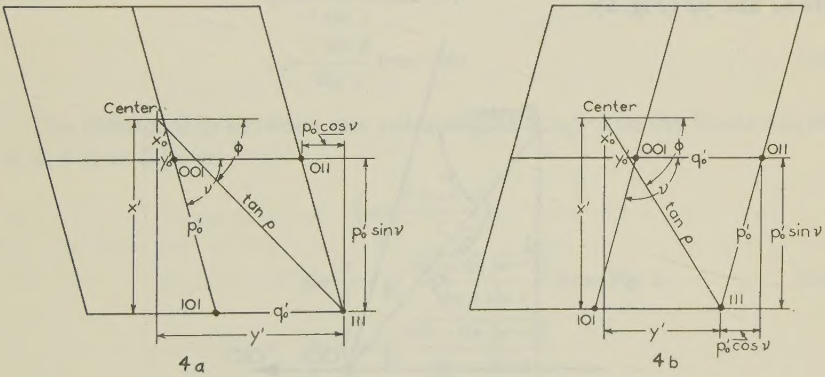

FIG. 4. Gnomonic Projection Constants in the Triclinic System with ν less than 90°00′ (4a) and greater than 90°00′ (4b).

Calculation of Projection Elements. The following formulae are useful in the calculation of the projection elements p_0', q_0', x_0', y_0', from two-circle goniometric measurements (see Fig. 4).

$$x'=\sin\phi\,\tan\rho=x_0'+\frac{h}{l}p_0'\,\sin\nu \text{ from Fig. 4}\ldots\ldots(11)$$

$$y'=\cos\phi\,\tan\rho=y_0'+\frac{k}{l}q_0'+\frac{h}{l}p_0'\,\cos\nu \text{ from Fig. 4}\ldots\ldots(12)$$

If x_1', x_2', . . . x_n' are the ordinates and y_1', y_2', . . . y_n' the abscissae of the gnomonic poles $(h_1k_1l_1)$, $(h_2k_2l_2)$, . . . $(h_nk_nl_n)$, then:

$$p_0'\sin\nu=\frac{l_1l_2(x_1'-x_2')}{h_1l_2-h_2l_1} \text{ from (11)}\ldots\ldots(13)$$

$$x_0'=x'-\frac{h}{l}p_0'\,\sin\nu \text{ from (11)}\ldots\ldots(14)$$

$$p_0'\cos\nu=\frac{l_1l_2(y_1'-y_2')(k_2l_3-k_3l_2)-l_2l_3(y_2'-y_3')k_1l_2-k_2l_1}{(h_1l_2-h_2l_1)(k_2l_3-k_3l_2)-(h_2l_3-h_3l_2)(k_1l_2-k_2l_1)}\ldots\ldots(15)$$

$$q_0'=\frac{p_0'\cos\nu(h_2l_1-h_1l_2)+l_1l_2(y_1'-y_2')}{k_1l_2-k_2l_1} \text{ from (12)}\ldots\ldots(16)$$

$$y_0'=y'-\frac{k}{l}q_0'-\frac{h}{l}p_0'\,\cos\nu \text{ from (12)}\ldots\ldots(17)$$

$$\tan\nu=\frac{p_0'\sin\nu}{p_0'\cos\nu}\ldots\ldots(18)$$

$$p_0'=\frac{p_0'\sin\nu}{\sin\nu}=\frac{p_0'\cos\nu}{\cos\nu}\ldots\ldots(19)$$

Relation of Projection Elements to Polar Elements. ϕ_0 and ρ_0 are the azimuth and the polar distance of c(001), the rectangular coordinates of which are x_0' and y_0' (Fig. 5).

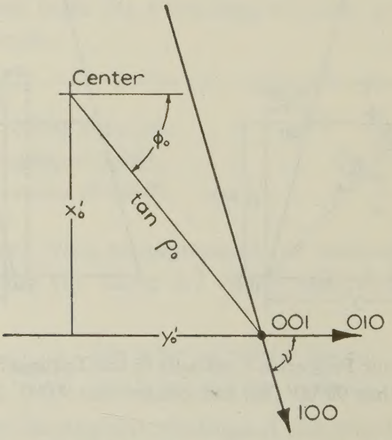

FIG. 5. Angular and Rectangular Coordinates of *c* (001) in the Triclinic System.

$$\tan\phi_0=\frac{x_0'}{y_0'} \text{ from Fig. 5}\ldots\ldots(20)$$

$$=\frac{x_0}{y_0}\text{ from Figs. 1 and 5}$$

(projection values are primed, and polar values are unprimed)

$$\tan\rho_0=\frac{x_0'}{\sin\phi_0}=\frac{y_0'}{\cos\phi_0}\text{ from Fig. 5}\tag{21}$$

$$\sin\rho_0=\frac{x_0}{\sin\phi_0}=\frac{y_0}{\cos\phi_0}\text{ from Fig. 1}\tag{22}$$

$$x_0=\sin\rho_0\sin\phi_0\tag{23}$$

$$y_0=\sin\rho_0\cos\phi_0\tag{24}$$

$$p_0=p_0'\cos\rho_0\text{ from Fig. 1}\tag{25}$$

$$q_0=q_0'\cos\rho_0\text{ from Fig. 1}\tag{26}$$

$$\cos\lambda=y_0\text{ from Fig. 2}\tag{27}$$

$$\cos\mu=y_0\cos\nu+x_0\sin\nu\text{ from Fig. 2}\tag{28}$$

The linear and polar elements are related as follows:

$$a:b(=1):c::\frac{\sin\alpha}{p_0}:\frac{\sin\beta}{q_0}:\frac{\sin\gamma}{r_0(=1)}::\frac{\sin\lambda}{p_0}:\frac{\sin\mu}{q_0}:\frac{\sin\nu}{r_0(=1)}\tag{29}$$

$$a=\frac{q_0'\sin\lambda}{p_0'\sin\mu}\text{ from (25), (26), (29)}\tag{30}$$

$$c=\frac{q_0'\cos\nu\sin\lambda}{\sin\mu}\text{ from (26) and (29)}\tag{31}$$

$$p_0=\frac{c\sin\alpha}{a\sin\gamma}\text{ from (29)}\tag{32}$$

$$q_0=\frac{c\sin\beta}{\sin\gamma}\text{ from (29)}\tag{33}$$

The relationship between the polar angles λ, μ, ν and the linear angles α, β, γ is as follows

$$\left(\sigma=\frac{\lambda+\mu+\nu}{2}\right):$$

$$\sin\frac{\alpha}{2}=\sqrt{\frac{\sin\sigma\sin(\sigma-\lambda)}{\sin\mu\sin\nu}}\text{ from Fig. 2}\tag{34}$$

$$\sin\frac{\beta}{2}=\sqrt{\frac{\sin\sigma\sin(\sigma-\mu)}{\sin\nu\sin\lambda}}$$

$$\sin\frac{\gamma}{2}=\sqrt{\frac{\sin\sigma\sin(\sigma-\nu)}{\sin\lambda\sin\mu}}$$

To obtain λ, μ, ν from α, β, γ, substitute the latter for the former, respectively, in (34).

Order of Form Listing. The following order of listing (Table 3) is used in the triclinic system. The letters c, b, a, m, M are reserved for the faces (001), (010), (100), (110), 1$\bar{1}$0), respectively.

TABLE 3. ORDER OF FORM LISTING IN THE TRICLINIC SYSTEM

Class	1		$\bar{1}$
Lower	Upper		
$\bar{c}$	c	001	001
	b	010	010
	$-b$	$0\bar{1}0$	
	a	100	100
	$-a$	$\bar{1}00$	
	d	$hk0$	$hk0$ in order of increasing $\frac{h}{k}$
	$-d$	$\bar{h}\bar{k}0$	
	D	$h\bar{k}0$	$h\bar{k}0$ in order of decreasing $\frac{h}{k}$
	$-D$	$\bar{h}k0$	
$\bar{w}$	w	$0kl$	$0kl$ in order of increasing $\frac{k}{l}$
$\bar{W}$	W	$0\bar{k}l$	$0\bar{k}l$ in order of increasing $\frac{k}{l}$
$\bar{e}$	e	$h0l$	$h0l$ in order of increasing $\frac{h}{l}$
$\bar{E}$	E	$\bar{h}0l$	$\bar{h}0l$ in order of increasing $\frac{h}{l}$
x	x*	hhl	hhl in order of increasing $\frac{h}{l}$
x	x	$h\bar{h}l$	$h\bar{h}l$ in order of increasing $\frac{h}{l}$
x	x	$\bar{h}hl$	$\bar{h}hl$ in order of increasing $\frac{h}{l}$
x	x	$\bar{h}\bar{h}l$	$\bar{h}\bar{h}l$ in order of increasing $\frac{h}{l}$
x	x	hkl	hkl in order of increasing $\frac{h}{l}$
x	x	$h\bar{k}l$	$h\bar{k}l$ in groups of equal $\frac{h}{l}$, list
x	x	$\bar{h}kl$	$\bar{h}kl$ in order of increasing $\frac{k}{l}$
x	x	$\bar{h}\bar{k}l$	$\bar{h}\bar{k}l$

* x indicates possible occurrence of form.

Triclinic Angles. The angles given in triclinic tables are: ϕ, ρ, A, B, C. Figure 6 is a stereographic projection showing these angles.

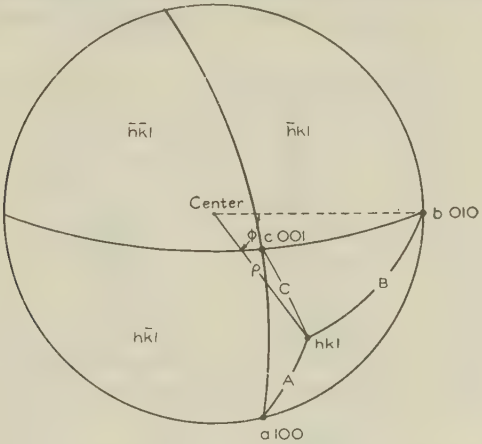

FIG. 6. Stereographic Projection of Angles Given for Forms in the Triclinic System.

$$\tan \phi_{hkl} = \frac{x'}{y'} = \frac{x'_0 + \frac{h}{l} p'_0 \sin \nu}{y'_0 + \frac{k}{l} q'_0 + \frac{h}{l} p'_0 \cos \nu} \text{ from Fig. 4} \ldots\ldots\ldots\ldots (35)$$

$$\tan \rho_{hkl} = \frac{x'}{\sin \phi} = \frac{y'}{\cos \phi} \text{ from Fig. 4 and (35)} \ldots\ldots\ldots\ldots (36)$$

The angles A, B, C, are the angles which the face makes with a (100), b (010), c (001), respectively. These angles are calculated by means of the general formula for the interfacial angle Δ:

$$\cos \Delta = \cos \rho_1 \cos \rho_2 + \sin \rho_1 \sin \rho_2 \cos (\phi_2 - \phi_1) \ldots\ldots\ldots\ldots (37)$$

where ϕ_1, ρ_1 and ϕ_2, ρ_2 are the angular coordinates of the two faces. For the specific cases of the calculations of the angles A, B, C, formula (37) becomes:

$$\cos A = \sin \rho_{hkl} \cos (\phi_{100} - \phi_{hkl}) \ldots\ldots\ldots\ldots (38)$$

$$\cos B = \sin \rho_{hkl} \cos \phi_{hkl} \ldots\ldots\ldots\ldots (39)$$

$$\cos C = \cos \rho_{hkl} \cos \rho_0 + \sin \rho_{hkl} \sin \rho_0 \cos (\phi_0 - \phi_{hkl}) \ldots\ldots\ldots\ldots (40)$$

A graphical check is always made to avoid gross errors. The only source of error in the determination of ϕ and ρ is the calculation of the x' and y' coordinates. These may be checked satisfactorily on a gnomonic projection with a unit circle radius of 10 cm., using the projection constants for plotting the faces. The interfacial angles A, B, C, are checked on a stereographic net (20 cm. radius), using the calculated ϕ and ρ values for plotting the faces. This check is accurate to ± 15 minutes.

THE MONOCLINIC SYSTEM

Elements. The elements here consist of: the linear axial ratio, $a:b:c$ ($b=1$), and the axial angle β between the positive ends of the c and a axes; the polar ratio, $p_0:q_0:r_0$ ($r_0=1$), and the reciprocal axial angle μ (the supplement of β); the polar ratio $r_2:p_2:q_2$ ($q_2=1$), obtained when b (010) is set in polar position, and the phi of a (100) is 0°00′; the projection constants p_0', q_0', x_0' (see Fig. 8).

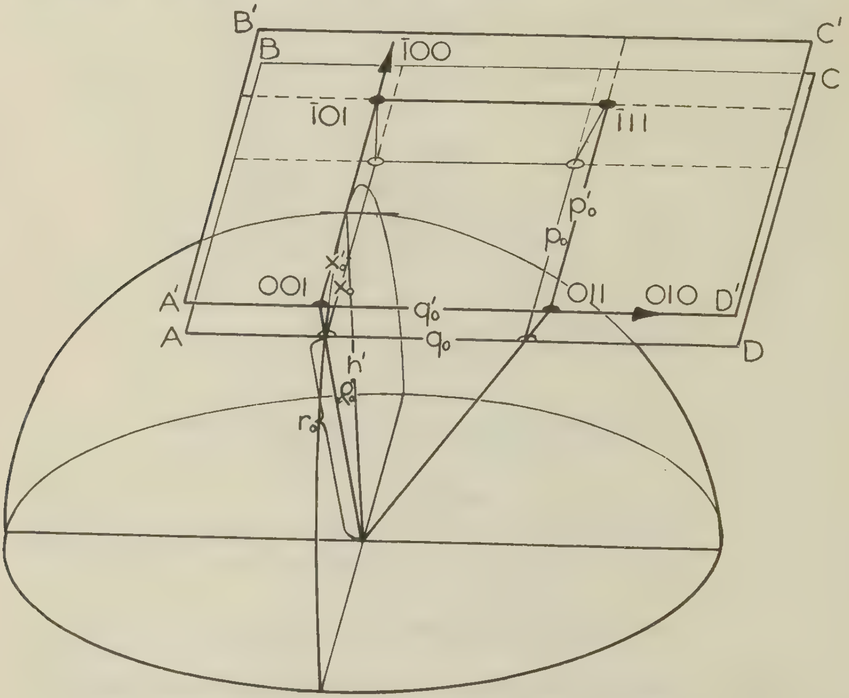

FIG. 7. Relation of Gnomonic Projection Elements to Polar Elements in the Monoclinic System.

In the monoclinic system, as in the triclinic, the projection elements do not coincide with the polar elements. For $r_0=1$ the gnomonic plane $A'B'C'D'$ (Fig. 7) must drop to the position of $ABCD$, the amount of that drop being a function of the ρ angle of c (001), (ρ_0).

Once the poles of measured faces have been plotted on the gnomonic projection and the correct gnomonic net drawn, the following convention is observed: $c<a$ (b is fixed by symmetry). If the lattice is primitive, the base is the node of the gnomonic net closest to the center of projection;

this yields the least anorthism of the axes. If the lattice is centered, the base is usually chosen in such a manner that the lattice is base-centered, whether or not this makes $c<a$.

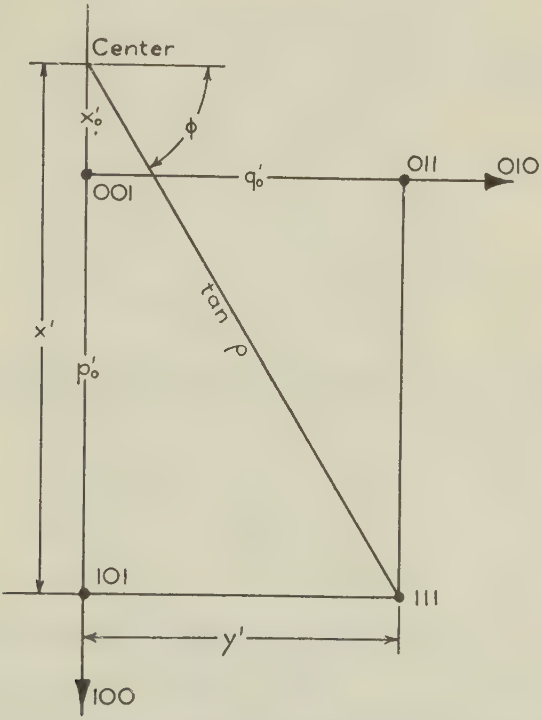

FIG. 8. Gnomonic Projection Constants in the Monoclinic System, Conventional Orientation.

Calculation of Projection Elements. The ϕ and ρ angles of the various faces are obtained from measurements. From Fig. 8 are derived the following:

$$x' = x_0' + \frac{h}{l} p_0' = \sin\phi \tan\rho \text{ (Fig. 8)} \ldots\ldots (41)$$

If x_1' and x_2' are the x' coordinates of faces $(h_1k_1l_1)$ and $(h_2k_2l_2)$, then:

$$p_0' = \frac{l_1l_2(x_1' - x_2')}{(h_1l_2 - h_2l_1)} \text{ (from 41)} \ldots\ldots (42)$$

$$x_0' = x' - \frac{h}{l} p_0' \text{ (from 41)} \ldots\ldots (43)$$

$$y' = \frac{k}{l} q_0' = \cos\phi \tan\rho \text{ (Fig. 8)} \ldots\ldots (44)$$

$$q_0' = \frac{ly'}{k} \text{ (from 44)} \tag{45}$$

$$\cot \mu = x_0' \tag{46}$$

$$\tan \rho_0 = x_0' \tag{47}$$

Calculation of Polar Elements. The polar elements are related to the projection elements as follows:

$$p_0 = p_0' \cos \rho_0 = p_0' \sin \mu \text{ (Fig. 7)} \tag{48}$$

$$q_0 = q_0' \cos \rho_0 = q_0' \sin \mu \text{ (Fig. 7)} \tag{49}$$

$$r_0 = 1 \tag{50}$$

$$r_2 = \frac{1}{q_0} = \frac{1}{q_0' \sin \mu} \tag{51}$$

$$p_2 = \frac{p_0}{q_0} = \frac{p_0'}{q_0'} \tag{52}$$

$$q_2 = 1 \tag{53}$$

Calculation of Linear Elements. The linear elements are related as follows to the polar and projection elements:

$$a = \frac{q_0}{p_0 \sin \mu} = \frac{q_0}{p_0 \sin \mu} \text{ (from 29)} \tag{54}$$

$$c = \frac{q_0}{\sin \mu} = q_0' \text{ (from 29)} \tag{55}$$

$$\beta = 180° - \mu \tag{56}$$

The derivation of the elements of a monoclinic mineral from measurements made with the *b*-axis vertical is as follows.

V_0 may be obtained as in (9) and (10). If, however, the quality of either *c* (001) or *a* (100) is sufficiently good, the vertical circle reading of one of them may be taken as V_0. The ϕ_2 readings for all of the faces are obtained by subtracting V_0 from their vertical circle readings (see Peacock—*Am. Jour. Sci.*, **28**, 241–254, for meaning of subscript $_2$). Ordinarily, the elements are calculated with the azimuth ϕ_2 of (100) = 0°00′ (Fig. 9), and the angles are given accordingly; but they may be calculated as readily when the azimuth of (001) = 0°00′. Two sets of similar formulae are given below for these two cases. Using the measured ϕ_2 and ρ_2 values, the x and y coordinates of each face in this orientation are obtained by (11) and (12). In the formulae below x_1 and x_2 are the ordinates and y_1 y_2 are the abscissae of any two gnomonic poles $(h_1k_1l_1)$ $(h_2k_2l_2)$. Indices obtained from the gnomonic plot in this orientation are listed in the sequence of the intercepts of the gnomonic pole on the polar axes p_2, $q_2 = 1$, and r_2, clearing fractions where necessary. Thus, these indices are identical with those obtained for the same face in the normal position where $r_0 = 1$.

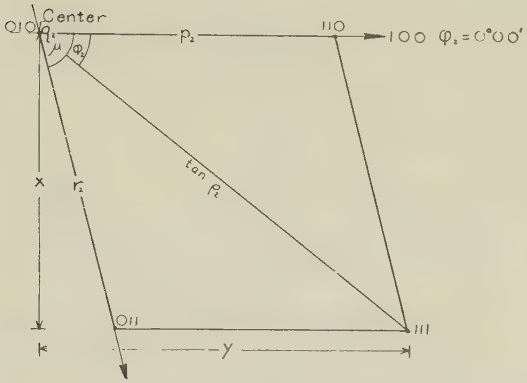

FIG. 9. Gnomonic Projection Constants in the Monoclinic System with *b*-axis vertical.

where ϕ_2 of *a* (100)=0°00′

$$\tan\mu=\frac{k_1h_2x_1-k_2h_1x_2}{k_1h_2y_1-k_2h_1y_2}\quad(57)$$

$$r_2=\frac{kx}{l\sin\mu}\quad(58)$$

$$p_2=\frac{ky}{h}-\frac{kx}{h\tan\mu}\quad(59)$$

where ϕ_2 of *c* (001)=0°00′

$$\tan\mu=\frac{k_1l_2x_1-k_2l_1x_2}{k_1l_2y_1-k_2l_1y_2}\quad(60)$$

$$r_2=\frac{ky}{l}-\frac{kx}{l\tan\mu}\quad(61)$$

$$p_2=\frac{kx}{h\sin\mu}\quad(62)$$

$$a=\frac{1}{p_2\sin\mu},\quad c=\frac{1}{r_2\sin\mu}\quad(63)$$

$$p_0'=\frac{p_2}{r_2\sin\mu},\quad q_0'=\frac{1}{r_2\sin\mu},\quad x_0'=\cot\mu\quad(64)$$

Order of Form Listing. The order of listing in the monoclinic system is shown in Table 4. The letters *c*, *b*, *a*, *m* are conventionally used for (001), (010), (100), (110), respectively.

Monoclinic Angles. The angles given in the monoclinic system are ϕ, ρ, ϕ_2, $\rho_2=B$, C, A (Fig. 10). ϕ_2 and ρ_2 are the phi and rho values obtained when *b*(010) is set in polar position and the azimuth of *a*(100) is 0°00′ (in this position the $r_2:p_2:q_2$ polar ratio is obtained). *C* and *A* represent the angles which a face makes with *c*(001) and *a*(100), respectively,

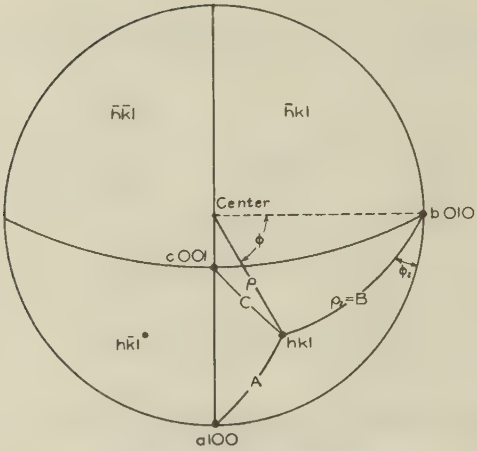

FIG. 10. Stereographic Projection of Angles Given in the Monoclinic System.

$$\tan \phi = \frac{x'}{y'}, \text{(from Fig. 8)} \qquad (65)$$

$$\tan \rho = \frac{x'}{\sin \phi} = \frac{y'}{\cos \ \phi} \text{ (from Fig. 8)} \qquad (66)$$

$$\cot \phi_2 = x' = \sin \phi \tan \rho \text{ from (41), Fig. 9, Fig. 10} \qquad (67)$$

$$\cos \rho_2 = \cos B = \sin \rho \cos \phi \text{ from Fig. 9, Fig. 10} \qquad (68)$$

$$\cos C = \sin (\phi_2 + \rho_0) \sin B \text{ from Fig. 10} \qquad (69)$$

$$\cos A = \sin \rho \sin \phi \text{ from Fig. 10} \qquad (70)$$

TABLE 4. ORDER OF FORM LISTING IN THE MONOCLINIC SYSTEM

Class	m		2		$\frac{2}{m}$
Lower	Upper				
x	c	001		001	001
	b	010		010	010
			$-b$	$0\bar{1}0$	
	a	100		100	100
	$-a$	$\bar{1}00$			
	k	$hk0$	k'	$hk0$	$hk0$ in order of increasing phi
	$-k$	$\bar{h}k0$	$'k$	$h\bar{k}0$	
x	w	$0kl$	w'	$0kl$	$0kl$ in order of increasing rho
			$'w$	$0\bar{k}l$	

TABLE 4. *Continued*

Class	m	2	$\frac{2}{m}$
Lower	Upper		
x	d $h0l$	$h0l$	$h0l$ in order of increasing $\frac{h}{l}$
x	D $\bar{h}0l$	$\bar{h}0l$	$\bar{h}0l$ in order of increasing $\frac{h}{l}$
x	q hhl	hhl	hhl in order of increasing $\frac{h}{l}$
x	Q $\bar{h}hl$	$\bar{h}hl$	$\bar{h}hl$ in order of increasing $\frac{h}{l}$
x	r hkl	r' hkl $'r$ $h\bar{k}l$	hkl in order of increasing $\frac{h}{l}$; in groups of equal $\frac{h}{l}$, list in order of increasing $\frac{k}{l}$
x	R $\bar{h}kl$	R' $\bar{h}kl$ $'R$ $\bar{h}\bar{k}l$	$\bar{h}kl$ same as for hkl

THE ORTHORHOMBIC SYSTEM

Elements. The elements in the orthorhombic system include: the axial ratio $a:b:c$ $(b=1)$ (with the convention usually adopted that $c<a<b$); the polar ratio $p_0:q_0:r_0$ $(r_0=1)$; the polar ratio $q_1:r_1:p_1$ $(p_1=1)$; the polar ratio $r_2:p_2:q_2$ $(q_2=1)$ (See Peacock—*Am. Jour. Sci.*, **28,** 241–254 [1934]. See, also, Fig. 11). Cyclic permutations of the polar ratio are given because an orthorhombic crystal may be measured with any one of the three axes vertical, and the ensuing gnomonic plot would change accordingly.

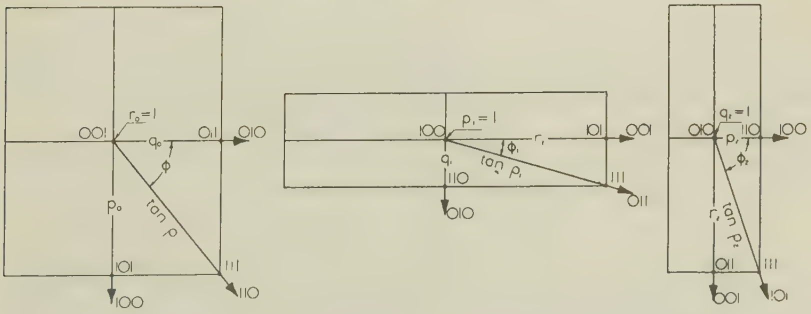

FIG. 11. Gnomonic Projections of Cyclic Permutations of Polar Elements in the Orthorhombic System (Polar Elements of Cannizzarite).

Calculation of Elements. The angular measurements, ϕ and ρ, are related to the linear and polar elements as follows:

$$a=\frac{q_0}{p_0}=\frac{k\cot\phi}{h}\text{ (Fig. 11)}\ldots\ldots(71)$$

$$p_0=\frac{l\sin\phi\tan\rho}{h}\text{ (Fig. 11)}\ldots\ldots(72)$$

$$q_0=c=\frac{l\cos\phi\tan\rho}{k}\text{ (Fig. 11)}\ldots\ldots(73)$$

Order of Form Listing. The order of listing in Table 5 is followed in the orthorhombic system. The letters c, b, a, m, are reserved for the faces (001), (010), (100), (110), respectively. The 90° meridian defines right and left forms (Fig. 12).

TABLE 5. ORDER OF FORM LISTING IN THE ORTHORHOMBIC SYSTEM

Class $m\ m\ 2$		$2\ 2\ 2$	$\frac{2}{m}\ \frac{2}{m}\ \frac{2}{m}$
Lower	Upper		
x	c 001	001	001
	b 010	010	010
	a 100	100	100
	k $hk0$	$hk0$	$hk0$ in order of increasing $\frac{h}{k}$
x	w $0kl$	$0kl$	$0kl$ in order of increasing $\frac{k}{l}$
x	d $h0l$	$h0l$	$h0l$ in order of increasing $\frac{h}{l}$
x	q hhl	q' hhl $'q$ $h\bar{h}l$	hhl in order of increasing $\frac{h}{l}$
x	r hkl	r' hkl $'r$ $h\bar{k}l$	hkl in order of increasing $\frac{h}{l}$; in groups of equal $\frac{h}{l}$, list in order of increasing $\frac{k}{l}$

Orthorhombic Angles. Six angles for each form are given in the orthorhombic system. These are: ϕ and ρ in the conventional orientation $(c<a<b)$; ϕ_1 and $\rho_1=A$, with $a(100)$ in polar position and the phi of $c(001)$ equal to 0°00′; and ϕ_2 and $\rho_2=B$, with $b(010)$ in polar position and the phi of $a(100)$ equal to 0°00′ (see Fig. 12). Not only do these angles give important interfacial angles, but they also provide a ready check on measured angles regardless of which axis is made vertical.

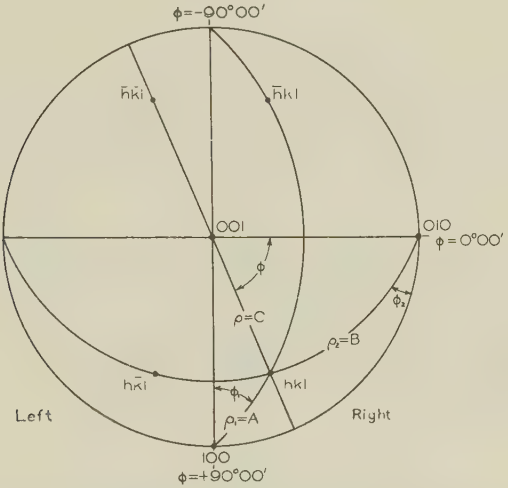

FIG. 12. Stereographic Projection Showing Form Designation and Angles in the Orthorhombic System.

$$\tan\phi=\frac{h\,p_0}{k\,q_0}\text{ from Fig. 11}\ldots\ldots(74)$$

$$\tan\rho=C=\frac{h\,p_0}{l\sin\phi}=\frac{k\,q_0}{l\cos\phi}\text{ from Fig. 11}\ldots\ldots(75)$$

$$\tan\phi_1=\frac{k\,q_0}{l}\text{ from Fig. 12}\ldots\ldots(76)$$

$$\cos\rho_1=\cos A=\sin\rho\sin\phi\text{ from Fig. 12}\ldots\ldots(77)$$

$$\cot\phi_2=\frac{h\,p_0}{l}\text{ from Fig. 12}\ldots\ldots(78)$$

$$\cos\rho_2=\cos B=\sin\rho\cos\phi\text{ from Fig. 12}\ldots\ldots(79)$$

TETRAGONAL SYSTEM

Elements. The elements in this system include the linear ratio, $a:c$ $(a=1)$, and the polar ratio $p_0:r_0$ $(r_0=1)$. In this case c and p_0 are equal and may be obtained from the ϕ and ρ readings of the various types of forms as follows:

$$\text{from } (0kl) \text{ or } (k0l)\ c=p_0=\frac{l\tan\rho}{k}\ \ldots\ldots\ldots\ldots\ (80)$$

$$\text{from } (hhl)\ c=p_0=\frac{l\tan\rho\sin 45^\circ}{h}\ \ldots\ldots\ldots\ldots\ (81)$$

$$\text{from } (hkl)\ c=p_0=\frac{l\tan\rho\sin\phi}{h}=\frac{l\tan\rho\cos\phi}{k}\ \ldots\ldots\ (82)$$

Order of Form Listing. Table 6 shows the order in the tetragonal system. The letters c, a, m, are reserved for the faces (001), (010), (110), respectively. The plus 45° and minus 45° meridians define right and left forms (Fig. 13).

TABLE 6. ORDER OF FORM LISTING IN THE TETRAGONAL SYSTEM

Class $\bar{4}$		4		$\frac{4}{m}$	$\bar{4}\,2\,m$	$4\,m\,m$		$4\,2\,2$	$\frac{4}{m}\,\frac{2}{m}\,\frac{2}{m}$
		Lower	Upper			Lower	Upper		
c	001	x	001	001	001	x	001	001	001
a	010		010	010	010		010	010	010
m	110		110	110	110		110	110	110
d	$hk0$		$hk0$	$hk0$	$hk0$		$hk0$	$hk0$	$hk0$ in order of increasing $\frac{h}{k}$
$-d$	$\bar{h}k0$		$\bar{h}k0$	$\bar{h}k0$					
i'	$0kl$	x	$0kl$	$0kl$	$0kl$	x	$0kl$	$0kl$	$0kl$ in order of increasing $\frac{k}{l}$
$'i$	$k0l$								
o	hhl	x	hhl	hhl	hhl	x	hhl	hhl	hhl in order of increasing $\frac{h}{l}$
$-o$	$\bar{h}hl$				$\bar{h}hl$				
u'	hkl	x	hkl	hkl	hkl	x	hkl	hkl	hkl in order of increasing $\frac{h}{l}$;
$'u$	khl	x	khl	khl				khl	in groups of equal $\frac{h}{l}$, list
$-'u$	$\bar{h}kl$				$\bar{h}kl$				in order of increasing $\frac{k}{l}$
$-u'$	$\bar{k}hl$								

Tetragonal Angles. The angles given in the tetragonal system are: ϕ; ρ; A, the angle to $a(100)$; $\overline{M}$, the angle to $-m(1\bar{1}0)$, given for plus forms only; M, the angle to $m(110)$, given for minus forms only. These yield useful interfacial angles as is seen in Fig. 13. The formulae for calculation of these angles are:

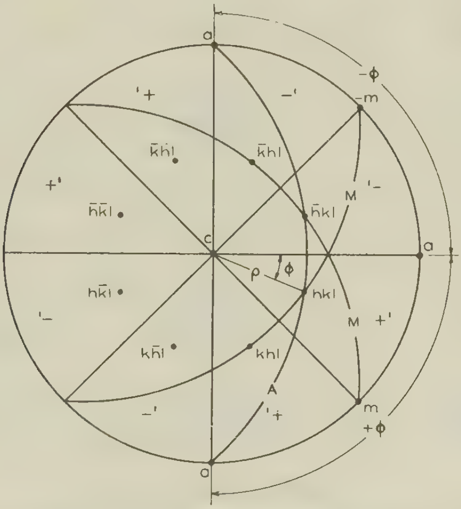

FIG. 13. Stereographic Projection Showing Form Designation and Angles in the Tetragonal System.

$\tan\phi=\dfrac{h}{k}$ from Fig. 13 .... (83)

$\tan\rho=\dfrac{hp_0}{l\sin\phi}=\dfrac{kp_0}{l\cos\phi}$ from Fig. 13 .... (84)

$\cos A=\sin\rho\sin\phi$; supplement is obtained when ϕ is negative, that is, for $\{\bar{h}kl\}$ and $\{\bar{k}hl\}$ forms .... (85)

$\cos M=\sin\rho\cos(45°+\phi)$; supplement is obtained when form symbol is $\{khl\}$ .... (86)

$\cos M=\sin\rho\cos(45°-\phi)$; supplement is obtained when form symbol is $\{\bar{k}hl\}$ .... (87)

Since ϕ is a constant for each h/k value in the tetragonal system, the following table of ϕ angles is given with variations in h and k from 1 to 11. The angles are given according to increasing magnitude to facilitate rapid comparison with measured values. The same angles are valid in the isometric system.

TABLE 7. PHI ANGLES IN THE TETRAGONAL SYSTEM

$h:k$	ϕ	$h:k$	ϕ	$h:k$	ϕ
1:11	5°11′40″	4:11	19°58′59″	7:10	34°59′31″
1:10	5 42 38	3: 8	20 33 22	5: 7	35 32 16
1: 9	6 20 25	2: 5	21 48 05	8:11	36 01 39
1: 8	7 07 30	3: 7	23 11 55	3: 4	36 52 12
1: 7	8 07 48	4: 9	23 57 43	7: 9	37 52 30
1: 6	9 27 44	5:11	24 26 38	4: 5	38 39 35
2:11	10 18 17	1: 2	26 33 54	9:11	39 17 22
1: 5	11 18 36	6:11	28 36 38	5: 6	39 48 20
2: 9	12 31 44	5: 9	29 03 17	6: 7	40 36 05
1: 4	14 02 10	4: 7	29 44 42	7: 8	41 11 09
3:11	15 15 18	3: 5	30 57 50	8: 9	41 37 37
2: 7	15 56 44	5: 8	32 00 19	9:10	41 59 14
3:10	16 41 57	7:11	32 28 16	10:11	42 16 25
1: 3	18 26 06	2: 3	33 41 24	1: 1	45 00 00

HEXAGONAL SYSTEM

Introduction. The hexagonal system has caused considerable difficulty, principally due to the introduction of the so-called G_2 position of V. Goldschmidt. The G_1 position is, however, without ambiguity, as has been pointed out by Peacock (*Am. Mineral.*, **23,** 314–328, 1938) if certain changes of the polar axes and prime meridian of Goldschmidt are made. In Goldschmidt's works the G_2 position is sometimes the only one used. It is important, therefore that the transformation from the G_2 Bravais symbol to the G_1 Bravais symbol be given. It is as follows:

$$\begin{array}{ccccccc} h & & k & & \bar{i} & & l \\ \frac{1}{3}\ \frac{2}{3}\ 0\ 0 & / & \frac{1}{3}\ \frac{\bar{1}}{3}\ 0\ 0 & / & \bar{i} & / & 0001 \end{array} \qquad (88)$$

where i equals $(h+k)$.

Elements. The elements of the hexagonal system include the axial ratio, $a:c$ $(a=1)$, and the polar ratio, $p_0:r_0$ $(r_0=1)$. Some of the more important mathematical relations here involved are as follows:

$$p_0 = \text{tangent } \rho\ (10\bar{1}1) \qquad (89)$$

$$c = \frac{p_0}{2}\sqrt{3} = \text{tangent } \rho\ (11\bar{2}2) \qquad (90)$$

The elements p_0 or c may be obtained from the ϕ and ρ angles of faces intersecting three axes or more, one of which must be the c-axis, by the following formulae:

$$\text{from } (h0\bar{h}l) \text{ or its equivalents, } p_0=\frac{l\tan\rho}{h};\ c=\frac{l\sqrt{3}\tan\rho}{2h}\ldots\ldots\ldots\ldots(91)$$

$$\text{from } (hh\,\bar{2}\bar{h}\,l) \text{ or equivalents, } p_0=\frac{l\tan\rho}{h\sqrt{3}};\ c=\frac{l\tan\rho}{2h}\ldots\ldots\ldots\ldots\ldots(92)$$

$$\text{from } (hk\bar{i}l) \text{ or equivalents, } p_0=\frac{l\tan\rho}{\sqrt{h^2+k^2+hk}};\ c=\frac{l\sqrt{3}\tan\rho}{2\sqrt{h^2+k^2+hk}}\ldots(93)$$

Form Symbols. The four-index Bravais symbols are used throughout. When the lattice mode is rhombohedral, Millerian three index symbols are also given. Bravais *hkīl* symbols may be transformed to Millerian ***hkl*** symbols by the use of the following formula:

$$\text{Bravais to Miller: } \frac{1}{3}\;0\;\frac{\bar{1}}{3}\;\frac{1}{3}\Big/\frac{\bar{1}}{3}\;\frac{1}{3}\;0\;\frac{1}{3}\Big/0\;\frac{\bar{1}}{3}\;\frac{1}{3}\;\frac{1}{3}\ldots\ldots(94)$$

The reverse transformation is as follows:

$$\text{Miller to Bravais: } 1\;\bar{1}\;0\;/\;0\;1\;\bar{1}\;/\;\bar{1}\;0\;1\;/\;1\;1\;1\ldots\ldots\ldots\ldots(95)$$

Indexing of Forms. In the indexing of forms in the hexagonal system, two coordinate axes, P_1 and P_2 (Fig. 14), are used which are normal to $(10\bar{1}0)$ and $(01\bar{1}0)$, respectively (see also Fig. 15). The positive unit lengths along these coordinate axes extend from the center of projection to the gnomonic poles of $(10\bar{1}1)$ and $(01\bar{1}1)$. The Bravais indices $(hk\bar{i}l)$ are found as follows:

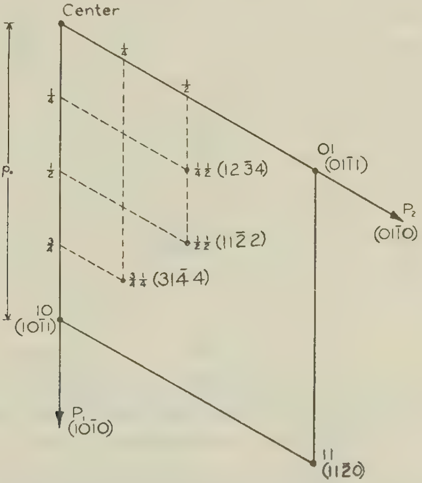

FIG. 14. Determination of Bravais Form Indices from the Gnomonic Projection in the Hexagonal System.

$h=P_1$ coordinate
$k=P_2$ coordinate
$\bar{i}=(h+k)$
$l=1$
(clearing fractions, if necessary)

In figure 14 the faces for which P_1 and P_2 coordinates are given receive the following indices:

$$\frac{1}{4}\ \frac{1}{2}=\left(\frac{1}{4}\cdot\frac{2}{4}\cdot\frac{\bar{3}}{4}\cdot 1\right)=(12\bar{3}4)$$

$$\frac{1}{2}\ \frac{1}{2}=\left(\frac{1}{2}\cdot\frac{1}{2}\cdot\bar{1}\cdot 1\right)=(11\bar{2}2)$$

$$\frac{3}{4}\ \frac{1}{4}=\left(\frac{3}{4}\cdot\frac{1}{4}\cdot\bar{1}\cdot 1\right)=(31\bar{4}4)$$

Order of Form Listing. The order of listing in the hexagonal system is given in Tables 7*a*, 7*b*, and 8. Table 7*a* includes those symmetry classes in which the lattice mode is necessarily primitive hexagonal (P). Table 7*b* is the order of listing for the remaining classes if their lattice mode is primitive hexagonal. If, however, the lattice mode is rhombohedral (*R*), the order of listing for these same classes is given in Table 8. The division into three tables is necessary since certain forms which are complementary (or correlative) merohedral forms in the primitive lattice mode are actually holohedral in the rhombohedral lattice mode. For example, $0h\bar{h}l$ forms must be listed with their complementary $h0\bar{h}l$ forms if the lattice is primitive; but they are listed separately if the lattice is rhombohedral. The letters *c*, *m*, *a* are reserved for the faces (0001), $(10\bar{1}0)$, $(11\bar{2}0)$, respectively. The plus and minus 30° meridians define right and left forms (Fig. 15).

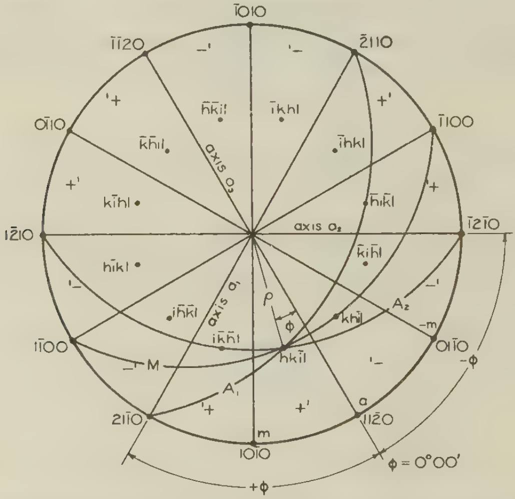

FIG. 15. Stereographic Projection Showing Form Designation and Angles in the Hexagonal System.

TABLE 7a. ORDER OF FORM LISTING IN CLASSES WITH LATTICE MODE UNIQUELY HEXAGONAL—*P*

Class $\bar{6}$		6		$\frac{6}{m}$	$\bar{6}\,m\,2$	6 *m m*		6 2 2	$\frac{6}{m}\,\frac{2}{m}\,\frac{2}{m}$
		Lower	Upper			Lower	Upper		
c	0001	x	x	x	x	x	x	x	x
m	$10\bar{1}0$		x	x	x		x	x	x
$-m$	$01\bar{1}0$				x				
a'	$11\bar{2}0$		x	x	x		x	x	x $(i>h>k)$
$'a$	$2\bar{1}\bar{1}0$								
j'	$hk\bar{i}0$		x	x	x		x	x	x in order of increasing $\frac{h}{k}$
$'j$	$i\bar{k}\bar{h}0$		x	x					
$-'j$	$kh\bar{i}0$				x				
$-j'$	$\bar{k}i\bar{h}0$								
q	$h0\bar{h}l$	x	x	x	x	x	x	x	x in order of increasing $\frac{h}{l}$
$-q$	$0h\bar{h}l$				x				
e'	$hh\,\bar{2h}\,l$	x	x	x	x	x	x	x	x in order of increasing $\frac{h}{l}$
$'e$	$2h\,\bar{h}\bar{h}\,l$								
s'	$hk\bar{i}l$	x	x	x	x	x	x	x	x in order of increasing $\frac{h}{k}$;
$'s$	$i\bar{k}\bar{h}l$	x	x					x	in groups of equal $\frac{h}{k}$,
$-'s$	$kh\bar{i}l$				x				list in order of increasing
$-s'$	$\bar{k}i\bar{h}l$								$\frac{h}{l}$.

TABLE 7b. ORDER OF FORM LISTING IN CLASSES WITH LATTICE MODE NOT UNIQUELY HEXAGONAL—*P*

Class 3			$\bar{3}$	3 *m*		3 2	$\bar{3}\,\frac{2}{m}$
Lower	Upper			Lower	Upper		
x	c	0001	x	x	x	x	x
	m	$10\bar{1}0$	x		x	x	x
	$-m$	$01\bar{1}0$			x		
	a'	$11\bar{2}0$	x		x	x	x
	$'a$	$2\bar{1}\bar{1}0$				x	$(i>h>k)$

TABLE 7*b*. *Continued*

Class 3			$\bar{3}$	$3m$		$3\ 2$	$\bar{3}\,\frac{2}{m}$
Lower		Upper		Lower	Upper		
	j'	$hk\bar{i}0$	x		x	x	x in order of increasing $\frac{h}{k}$
	$'j$	$i\bar{k}\bar{h}0$	x			x	
	$-'j$	$kh\bar{i}0$	x		x		
	$-j'$	$\bar{k}i\bar{h}0$	x				
x	q	$h0\bar{h}l$	x	x	x	x	x in order of increasing $\frac{h}{l}$
x	Q	$0h\bar{h}l$	x	x	x	x	x
x	e'	$hh\bar{2}\bar{h}\,l$	x	x	x	x	x same as for $h0\bar{h}l$
x	$'e$	$2h\,\bar{h}\bar{h}\,l$	x			x	x
x	s'	$hk\bar{i}l$	x	x	x	x	x in order of increasing $\frac{h}{k}$;
x	$'s$	$i\bar{k}\bar{h}l$	x			x	in groups of equal $\frac{h}{k}$,
x	$-'s$	$kh\bar{i}l$	x	x	x	x	x list in order of increasing $\frac{h}{l}$.
x	$-s'$	$\bar{k}i\bar{h}l$	x			x	

TABLE 8. ORDER OF FORM LISTING IN CLASSES WITH LATTICE MODE NOT UNIQUELY HEXAGONAL—*R*

Class 3			$\bar{3}$	$3m$		$3\ 2$	$\bar{3}\,\frac{2}{m}$
Lower		Upper		Lower	Upper		
x	c	0001	x	x	x	x	x
	m	$10\bar{1}0$	x		x	x	x
	$-m$	$01\bar{1}0$			x		
	a'	$11\bar{2}0$	x		x	x	x
	$'a$	$2\bar{1}\bar{1}0$				x	$(i>h>k)$
	j'	$hk\bar{i}0$	x		x	x	x in order of increasing $\frac{h}{k}$
	$'j$	$i\bar{k}\bar{h}0$	x			x	
	$-'j$	$kh\bar{i}0$	x		x		
	$-j'$	$\bar{k}i\bar{h}0$	x				
x	q	$h0\bar{h}l$	x	x	x	x	x in order of increasing $\frac{h}{l}$

TABLE 8. *Continued*

Class 3			$\bar{3}$	$3\,m$		$3\,2$	$\bar{3}\,\frac{2}{m}$
Lower		Upper		Lower	Upper		
x	Q	$0h\bar{h}l$	x	x	x	x	x same as for $h0\bar{h}l$
x	e'	$hh\,\bar{2}\bar{h}\,l$	x	x	x	x	x same as for $h0\bar{h}l$
x	$'e$	$2h\,\bar{h}\bar{h}\,l$	x			x	
x	s'	$hk\bar{i}l$	x	x	x	x	x in order of increasing $\frac{h}{k}$;
x	$'s$	$i\bar{k}\bar{h}l$	x			x	in groups of equal $\frac{h}{k}$,
							list in order of increasing $\frac{h}{l}$.
x	$-'s$	$kh\bar{i}l$	x	x	x	x	x same as for $hk\bar{i}l$
x	$-s'$	$\bar{k}i\bar{h}l$	x			x	

Hexagonal System Angles. The angles given in the hexagonal system are: (Fig. 15) the azimuth angle ϕ with ϕ of $(11\bar{2}0)$ 0°00′; the polar angle ρ, equal to the interfacial angle to c (0001); M, the interfacial angle to $(1\bar{1}00)$, given for crystals of the primitive mode only; A_1, the interfacial angle to $(2\bar{1}\bar{1}0)$, given for crystals of the rhombohedral mode only; and A_2, the interfacial angle to $(\bar{1}2\bar{1}0)$. The following formulae are useful in calculating these angles.

$$\tan\phi = \frac{h-k}{h+k}\cdot\frac{1}{\sqrt{3}} \text{ or } \cot\phi = \frac{h+k}{h-k}\cdot\sqrt{3} \quad \text{(96)}$$

$$\text{for } (h0\bar{h}l) \text{ and } (0h\bar{h}l)\ \tan\rho = \frac{p_0 h}{l} \quad \text{(97)}$$

$$\text{for } (hh\,\bar{2}\bar{h}\,l)\ \tan\rho = \frac{p_0 h\sqrt{3}}{l}$$

$$\text{for } (hk\bar{i}l)\ \tan\rho = \frac{p_0}{l}\sqrt{h^2+k^2+hk}$$

TABLE 9. CALCULATION OF INTERFACIAL ANGLES IN THE HEXAGONAL SYSTEM (FIG. 15)

Form	M	A_1	A_2
$h0\bar{h}l$	$\cos M=\frac{\sin\rho}{2}$	$\cos A_1=\frac{\sqrt{3}}{2}\sin\rho$	90°00′
$0h\bar{h}l$	$\cos(180°-M)=\frac{\sin\rho}{2}$	90°00′	$\cos A_2=\frac{\sqrt{3}}{2}\sin\rho$
$hh\bar{2}\bar{h}l$	90°00′	$\cos A_1=\frac{\sin\rho}{2}$	$\cos A_2=\frac{\sin\rho}{2}$
$2h\bar{h}\bar{h}l$	$\cos M=\frac{\sqrt{3}}{2}\sin\rho$	$A_1=90°00'-\rho$	$\cos(180°-A_2)=\frac{\sin\rho}{2}$
$hk\bar{i}l$	$\cos M=\sin\rho\sin\phi$	$\cos A_1=\sin\rho\cos(60°-\phi)$	$\cos A_2=\sin\rho\cos(60°+\phi)$
$i\bar{k}\bar{h}l$	$\cos M=\sin\rho\cos(30°+\phi)$	$\cos A_1=\sin\rho\cos\phi$	$\cos(180°-A_2)$ $=\sin\rho\cos(60°+\phi)$
$kh\bar{i}l$	$\cos(180°-M)=\sin\rho\sin\phi$	$\cos A_1=\sin\rho\cos(60°+\phi)$	$\cos A_2=\sin\rho\cos(60°-\phi)$
$\bar{k}i\bar{h}l$	$\cos(180°-M)$ $=\sin\rho\cos(30°+\phi)$	$\cos(180°-A_1)$ $=\sin\rho\cdot\cos(60°+\phi)$	$\cos A_2=\sin\rho\cos\phi$

The letter ϕ in the above table always refers to the plus right position of the form.

Since ϕ is a constant for each h/k value in the hexagonal system, the following table of ϕ angles is given with variations in h and k from 1 to 11. The angles are given according to increasing magnitude to facilitate rapid comparison with measured values.

TABLE 10. PHI ANGLES IN THE HEXAGONAL SYSTEM

$h:k$	ϕ	$h:k$	ϕ	$h:k$	ϕ
1: 1	0°00′00″	3:2	6°35′12″	3:1	16°06′08″
11:10	1 34 29	11:7	7 18 40	10:3	17 16 10
10: 9	1 44 26	8:5	7 35 21	7:2	17 47 01
9: 8	1 56 42	5:3	8 12 48	11:3	18 15 30
8: 7	2 12 15	7:4	8 56 54	4:1	19 06 24
7: 6	2 32 35	9:5	9 22 01	9:2	20 10 25
6: 5	3 00 16	11:6	9 38 15	5:1	21 03 06
11: 9	3 18 16	2:1	10 53 36	11:2	21 47 12
5: 4	3 40 14	11:5	12 12 59	6:1	22 24 23
9: 7	4 07 40	9:4	12 31 11	7:1	23 24 48
4: 3	4 42 54	7:3	13 00 14	8:1	24 10 57
11: 8	5 12 31	5:2	13 53 52	9:1	24 47 29
7: 5	5 29 47	8:3	14 42 17	10:1	25 17 06
10: 7	5 49 03	11:4	15 04 45	11:1	25 41 36

Special Relations in Rhombohedral Lattices. In crystals with a rhombohedral lattice mode there are generally given, in addition to the regular hexagonal elements, the following constants:

a_{rh}, the absolute length of the rhombohedral edge, derived from x-ray measurements.
α, the interaxial angle of the direct rhombohedral lattice.
λ, the interaxial angle of the reciprocal rhombohedral lattice.

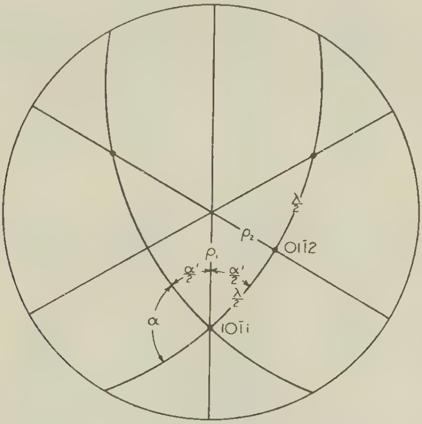

FIG. 16. Stereographic projection of Linear and Polar Interaxial Angles in the Rhombohedral Lattice Mode.

Some formulae relating the hexagonal and rhombohedral lattice modes follow (Fig. 16). If:

a_0 = absolute length along a-axis of hexagonal lattice
c_0 = absolute length along c-axis of hexagonal lattice
$\rho_1 = \rho$ of $(10\bar{1}1) = (0001) \wedge (10\bar{1}1)$
$\rho_2 = \rho$ of $(01\bar{1}2) = (0001) \wedge (01\bar{1}2)$

Then:

$$\sin\frac{\lambda}{2} = \frac{\sqrt{3}}{2}\sin\rho_1 = \sqrt{3}\sin\rho_2 \quad \text{(98)}$$

$$\cot\frac{\alpha'}{2} = \sqrt{3}\cos\rho_1 \quad \text{(99)}$$

primed values are supplements of unprimed

$$\cos\frac{\alpha'}{2} = \frac{\sqrt{3}}{2}\cos\rho_1 \quad \text{(100)}$$

$$\sin\frac{\alpha}{2} = \frac{a_0}{2a_{rh}} = \frac{3a_0}{2\sqrt{3a_0^2 + c_0^2}} = \frac{3}{2\sqrt{3 + \left(\frac{c}{a}\right)^2}} \quad \text{(101)}$$

$$a_{rh} = \frac{1}{3}\sqrt{3a_0^2 + c_0^2} \quad \text{(102)}$$

$$\frac{c_0}{a_0} = \sqrt{\left(\frac{3}{2 \sin \cdot \frac{\alpha}{2}}\right)^2 - 3} \quad \text{(103)}$$

$$\text{Volume rhombohedral cell} = \frac{a_0^2 \; c_0\sqrt{3}}{6} \quad \text{(104)}$$

Isometric System

Elements and angle tables are not given for isometric minerals, since the same angular relations hold for all. Angles for commonly found isometric forms are listed in Table 11. The meaning of the angles given is shown in Fig. 17.

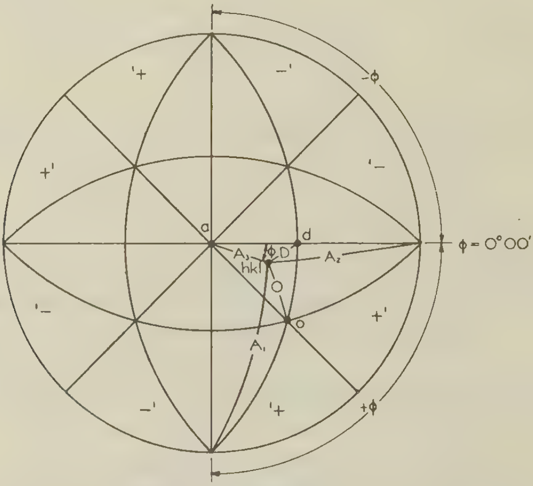

Fig. 17. Stereographic Projection Showing Form Designation and Angles in the Isometric System.

ϕ = azimuth angle measured from (010), zero meridian

$\rho = A_3$ = interfacial angle with (001)

A_1 = interfacial angle with (100)

A_2 = interfacial angle with (010)

D = interfacial angle with (011)

O = interfacial angle with (111)

Forms for which the same letters are used in all species are given letters in Table 11. In order that there may be sufficient remaining letters to designate the form assemblage of any one species, no convention has been adopted for the lettering of other forms.

TABLE 11. ISOMETRIC ANGLE TABLE

	Form	ϕ	$\rho = A_3$	A_1	A_2	D	O
a	001	—	0°00′	90°00′	90°00′	45°00′	54°44′
d	011	0°00′	45 00	90 00	45 00	0 00	35 16
o	111	45 00	54 44	54 44	54 44	35 16	0 00
	0·1·15	0 00	3 49	90 00	86 11	41 11	52 05
	0·1·10	0 00	5 42½	90 00	84 17½	39 17½	50 48½
	018	0 00	7 07½	90 00	82 52½	37 52½	49 52½
	017	0 00	8 08	90 00	81 52	36 52	49 13
	016	0 00	9 27½	90 00	80 32½	35 32½	48 22
	015	0 00	11 18½	90 00	78 41½	33 41½	47 12½
	029	0 00	12 31½	90 00	77 28½	32 28½	46 27½
h	014	0 00	14 02	90 00	75 58	30 58	45 33½
	072	0 00	15 56½	90 00	74 03½	29 03½	44 27½
	0·3·10	0 00	16 42	90 00	73 18	28 18	44 02
f	013	0 00	18 26	90 00	71 34	26 34	43 05½
k	025	0 00	21 48	90 00	68 12	23 12	41 22
	037	0 00	23 12	90 00	66 48	21 48	40 42
	049	0 00	23 57½	90 00	66 02½	21 02½	40 21
e	012	0 00	26 33	90 00	63 27	18 27	39 14½
	059	0 00	29 03½	90 00	60 56½	15 56½	38 16½
	047	0 00	29 44½	90 00	60 15½	15 15½	38 01½
l	035	0 00	30 58	90 00	59 02	14 02	37 37
g	023	0 00	33 41½	90 00	56 18½	11 18½	36 48½
	057	0 00	35 32½	90 00	54 27½	9 27½	36 21
ϑ	034	0 00	36 52	90 00	53 08	8 08	36 04
	045	0 00	38 39½	90 00	51 20½	6 20½	35 45½
	078	0 00	41 11	90 00	48 49	3 49	35 26½
	1·1·12	45 00	6 43½	85 15	85 15	40 28	48 00½
	1·1·11	45 00	7 19½	84 49½	84 49½	41 14½	47 24½
	1·1·10	45 00	8 03	84 19	84 19	39 38	46 41
	119	45 00	8 56	83 42	83 42	39 05½	45 48
	118	45 00	10 01½	82 56	82 56	38 26	44 42½
	117	45 00	11 25½	81 57	81 57	37 37	43 18½
	116	45 00	13 16	80 40	80 40	36 35	41 28

TABLE 11. *Continued*

	Form	ϕ	$\rho = A_3$	A_1	A_2	D	O
	115	45°00′	15°47½′	78°54½′	78°54½′	35°16′	38°56½′
	114	45 00	19 28½	76 22	76 22	33 33½	35 15½
	227	45 00	22 00	74 38½	74 38½	32 33	32 44
m	113	45 00	25 14½	72 27	72 27	31 29	29 29½
	338	45 00	27 56½	70 39	70 39	30 48	26 47½
	225	45 00	29 30	69 37½	69 37½	30 30	25 14
	337	45 00	31 13	68 33	68 33	30 15	23 31
n	112	45 00	35 16	65 54½	65 54½	30 00	19 28
	447	45 00	38 56½	63 36½	63 36½	30 12	15 47½
	335	45 00	40 19	62 46½	62 46½	30 23	14 25
β	223	45 00	43 19	60 59	60 59	30 58	11 25
	334	45 00	46 41	59 02½	59 02½	31 54½	8 03
	556	45 00	49 41	57 22½	57 22½	32 59½	5 03
	188	7 07½	45 13½	84 56	45 13½	5 04	30 12
	177	8 08	45 17½	84 14	45 17½	5 46	29 30
	166	9 27½	45 23½	83 16½	45 23½	6 43½	28 32½
	155	11 18½	45 33½	81 57	45 33½	8 03	27 13
ρ	144	14 02	45 52	79 58½	45 52	10 01½	25 14½
	277	15 56½	46 07½	78 34½	46 07½	11 25½	23 50½
q	133	18 26	46 30½	76 44	46 30½	13 16	22 00
	255	21 48	47 07½	74 12½	47 07½	15 47½	19 28½
p	122	26 34	48 11½	70 31½	48 11½	19 28½	15 47½
	355	30 58	49 23	67 00½	49 23	22 59½	12 16½
r	233	33 41½	50 14½	64 45½	50 14½	25 14½	10 01½
	344	36 52	51 20½	62 03½	51 20½	27 56½	7 19½
	455	38 39½	52 01	60 30	52 01	29 30	5 46
	1·6·12	9 27½	26 53	85 44	63 31	18 54½	35 22½
	1·6·11	9 27½	28 56½	85 26	61 29½	17 00½	34 14
	1·5·10	11 18½	27 01	84 53½	63 33	19 06½	34 37
	1·6·10	9 27½	31 18½	85 06	59 09½	14 51	33 01
	179	8 08	38 09½	84 59½	52 17½	8 42	30 57½
	128	26 34	15 37	83 05	76 04	31 39	40 08
	138	18 26	21 34	83 19½	69 35½	25 17	36 21

TABLE 11. *Continued*

	Form	ϕ	$\rho=A_3$	A_1	A_2	D	O
	148	14°02′	27°16′	83°37′	63°36½′	19°28½′	33°29½′
	158	11 18½	32 31	83 57	58 11½	14 18½	31 34½
	127	26 34	17 43	82 10½	74 12½	30 00	38 13
	137	18 26	24 18½	82 31	67 00½	22 59½	34 13½
	157	11 18½	36 04	83 22	54 44	11 32	29 56
	2·3·12	33 41½	16 43½	80 49	76 09	32 10	38 26
	156	11 18½	40 21½	82 42	50 35	8 57	28 22½
	2·5·11	21 48	26 05	80 36	65 54½	22 31	31 57
	125	26 34	24 05½	79 29	68 35	25 21	32 35½
	135	18 26	32 18½	80 16	59 32	17 01½	28 33½
	145	14 02	39 30½	81 07½	51 53	10 54	27 01
	239	33 41½	21 50	78 05½	71 58½	28 56	33 31
	249	26 34	26 25½	78 31½	66 33	23 50½	30 29½
	269	18 26	35 06	79 31½	56 56½	15 22	26 50½
	238	33 41½	24 15½	76 49½	70 00½	27 34½	31 12
t	124	26 34	29 12½	77 23½	64 07½	22 12½	28 07½
	134	18 26	38 19½	78 41½	53 57½	13 54	25 04
	3·5·11	30 58	27 55½	76 03½	66 19½	24 40	28 13½
	237	33 41½	27 15	75 17	67 36½	26 06	28 22½
	247	26 34	32 34½	76 04	61 13	20 33	25 22
	3·4·10	36 52	26 34	74 26	69 02	27 41½	28 37
	3·5·10	30 58	30 15	74 59	64 24½	23 37	26 08
	3·7·10	23 12	37 17½	76 11½	56 09½	17 00	23 16½
	236	33 41½	31 00	73 24	64 37½	24 37	24 52
s	123	26 34	36 42	74 30	57 41½	19 06½	22 12½
	358	30 58	36 05	72 21½	59 40	21 47	21 04
	235	33 41½	35 47½	71 04	60 52½	23 24½	20 31
	458	38 39½	38 40½	67 01½	60 47½	26 12	16 42
	346	36 52	39 48½	67 24½	59 11½	25 07½	16 03½
	234	33 41½	42 02	68 12	56 08½	23 12	15 13½
	345	36 52	45 00	64 54	55 33	25 50½	11 33½
	578	35 32½	47 04½	64 48½	53 25½	25 27½	10 36
	456	38 39½	46 47½	62 54½	55 18½	27 33½	9 19½

The order of form listing is given in Table 12 for the five isometric symmetry classes.

Calculation of Angles. The angles in Table 11 are calculated as follows:

$$\tan \phi = \frac{h}{k} \text{ (see Table 7)} \qquad (105)$$

$$\tan \rho = \frac{h}{l \sin \phi} = \frac{k}{l \cos \phi} \qquad (106)$$

$$\cos A_1 = \sin \rho \sin \phi \qquad (107)$$

$$\cos A_2 = \sin \rho \cos \phi \qquad (108)$$

$$\cos D = \frac{\sqrt{2}}{2}(\cos \rho + \sin \rho \cos \phi) \qquad (109)$$

$$\cos O = \cos \rho \cos 54°44' + \sin \rho \sin 54°44' \cos (45° - \phi) \qquad (110)$$

TABLE 12. ORDER OF FORM LISTING IN THE ISOMETRIC SYSTEM

Class	2 3	$\frac{2}{m}\bar{3}$	$\bar{4}\,3\,m$	4 3 2	$\frac{4}{m}\bar{3}\frac{2}{m}$	
a	001	*x*	*x*	*x*	*x*	
d	011	*x*	*x*	*x*	*x*	$(h<k<l)$
o	111	*x*	*x*	*x*	*x*	
$-o$	$\bar{1}11$		*x*			
e'	$0kl$	*x*	*x*	*x*	*x*	in order of increasing $\frac{k}{l}$
$'e$	$k0l$	*x*				
j	hhl	*x*	*x*	*x*	*x*	in order of increasing $\frac{h}{l}$
$-j$	$\bar{h}hl$		*x*			
n	hll	*x*	*x*	*x*	*x*	in order of increasing $\frac{h}{l}$
$-n$	$\bar{h}ll$		*x*			
s'	hkl	*x*	*x*	*x*	*x*	in order of increasing $\frac{h}{l}$;
$'s$	khl	*x*				in groups of equal $\frac{h}{l}$,
$-'s$	$\bar{h}kl$		*x*	*x*		list in order of increasing $\frac{k}{l}$.
$-s'$	$\bar{k}hl$					

ACKNOWLEDGMENTS

Valuable suggestions and criticisms relative to the manuscript have been given by Professors Charles Palache and Harry Berman of Harvard University and by Professor J. D. H. Donnay of Laval University. Professor M. A. Peacock of the University of Toronto has been of considerable help in the formulation of some of the procedures described in this paper. I wish to express my appreciation, here, for the assistance given by each of these men. The figures have been drawn from my sketches by Howard T. Evans.

OCCURRENCE OF WILLEMITE

Frederick H. Pough,
The American Museum of Natural History, New York, N. Y.

Abstract

Willemite (Zn_2SiO_4) is often considered, because of its importance at Franklin, N. J., to be characteristic of deposition under conditions of high temperature. By far the largest majority of occurrences, however, including seven new localities, indicate a formation through secondary alteration of ore minerals, often under arid climatic conditions. A number of alternatives are proposed to explain the formation of willemite as a mineral formed under unusual weathering conditions. An attempt is made to find a factor common to both hydrothermal and epithermal deposition, and to call attention to probable other occurrences which have been overlooked because of the inconspicuous appearance of most of the epithermal deposits.

The outstanding importance of willemite as an ore mineral at Franklin, New Jersey, together with the beautiful and varied appearance of the specimens and crystals found there and displayed in most collections throughout the world, has led to a general misconception of the manner of occurrence of this mineral, and of the conditions under which it forms. Willemite is not an uncommon mineral, it has been found in many places, but few collections display or have specimens from localities other than Franklin, New Jersey; Morésnet, Belgium; Salida, Colorado; and sometimes Musartut, Greenland.

This condition exists despite the fact that Spencer (1927) has described four occurrences, Clark (1916) one, Lindgren (1905–1919) three, Foshag (1934) one, Genth (1887) one, LaCroix (1910–13) six, and Pough (1940) one. Franklin specimens are far more showy than those from any other locality, and willemite is more abundant there than elsewhere, so there is some justification for the emphasis placed on the New Jersey occurrence. Furthermore, Franklin willemite is one of the finest minerals known for its display of fluorescence, and that, in this day of fluorescent lights and the popularization of mineralogy's spectacular aspects, has not detracted from the Franklin fame.

Consequently, the remainder of the world's willemite is blanketed by this competition and goes largely unsung. While many minerals reach their apogee at one particular place, such as Japanese stibnite, and epidote from Untersulzbachtal; we also think of Alaskan epidote and of Nevadan or Hungarian stibnite in an afterthought. No mineral needs to have its other localities pointed out so badly, for generally, no such afterthought follows in willemite's train, and this has led to widespread misunderstanding of willemite's place in a genetic series and its usual manner of formation.

TABLE 1

	Locality	Origin	Habit	a $11\bar{2}0$	m $10\bar{1}0$	Others	c 0001	e 0112	p $10\bar{1}1$	Others	Remarks	Authority
1	Morésnet, Belgium	Supergene	Prismatic	√			√	√			Small simple crystals	Lévy 1830
2	Franklin, N. J.	Hypogene	Prismatic and Tabular	√	√	√	√	√	√	√	Very varied in occurrence	
3	Socorro, N. M.	Supergene!	Prismatic	√	√	√	√	√	√	√	Associated with barite, wulfenite, mimetite, cerussite and quartz	Genth 1887 Penfield 1894
4	Salida, Colorado	?	Tabular	√	√	√	√	√				Penfield 1894
5	Morenci, Arizona	Supergene	Prismatic	√			√	√			With hemimorphite, dioptase and chrysocolla	Lindgren and Hillebrand 1904
6	Musartut, Greenland	Hypogene!		√	√	√	√	√	√	√	In quartz dike in sandstone	Bøggild 1905
7	Oslo, Norway	Hypogene	Prismatic	√	√	√	√	√	√	√	Contact metamorphic deposit. Skarn minerals, zeolites etc.	Goldschmidt 1911
8	Tchicoumba, French Congo	Supergene!	Prismatic	√	√	√	√	√	√		With wulfenite, quartz, Etc.	Lacroix 1910
9	Pimbi, French Congo	Supergene!	Prismatic	√				√			With wulfenite, cerussite, Etc.	Lacroix 1910
10	Djoué Mine, French Congo	Supergene!	Prismatic	√				√			With cerussite, dioptase, Etc.	Lacroix 1913
11	St. Pierre, Martinique	Hypogene	Prismatic								Formed on zinc objects at time of eruption of Mt. Pelé	Lacroix 1910
12	Constantine, Algeria	Supergene	Prismatic	√				√			With hematite, hemimorphite, calcite, and malachite	Lacroix 1910
13	Djebel Ressas, Algeria	?	Prismatic									Lacroix 1910
14	Cho-Dan, French Indo-China	?	Prismatic	√				√				Lacroix 1913
15	Beaver Co., Utah	Supergene	Prismatic	√	√		√	√			With hemimorphite, cerussite, mimetite, quartz, and calcite	Clark 1916
16	Broken Hill, No. Rhodesia	?	Prismatic	√				√			Over 100,000 tons massive in bones with hematite, limonite, goethite, and quartz	Buttgenbach Spencer 1927
17	Sable Antelope, No. Rhodesia	?	Prismatic	√				√			Hematite and Mn oxides	Spencer 1927
18	Lusaka, No. Rhodesia	?	Prismatic									Spencer 1927
19	Guchab, S.W. Africa	Supergene!	Prismatic	√				√			Malachite and chalcocite	Spencer 1927
20	Penoles, Durango, Mexico	Supergene!										Spencer 1927
21	Sinaloa, Mexico	Supergene!										Spencer 1927
22	Lubi, Belgian Congo	Supergene!	Prismatic	√			√	√		√	With dioptase, volborthite, barite and cerussite	Buttgenbach 1927
23	Balmat, New York	Supergene	Tabular	√	√	√	√	√	√	√	Constant in habit and occurrence	Brown 1936

Just as the Franklin willemites are unusual, so is the Franklin occurrence. Let us summarize the described occurrences of willemite given in Table 1. We see there that Franklin, Oslo, and Musartut are probably all the result of high temperature processes. But all the others seem secondary, formed as the result of the alteration of primary zinc sulphide ores, or secondary hemimorphite. This inevitably forces us to the conclusion that hypogene formation of willemite is not customary and that such occurrences are unusual.

That is only a first step however, for we still cannot say that the formation of willemite by alteration processes is the usual procedure, for clearly it is not. Hemimorphite is the common product of the oxidation of sphalerite when siliceous solutions are available; smithsonite when a carbonate radical is present. We still have the problem of the formation of the anhydrous silicate. As shown by innumerable occurrences, under very varied conditions, hemimorphite is the abundant silicate of zinc. It forms under all types of supergene conditions; at Franklin, at Joplin, and in New Mexico. We have then the problem of why willemite should form at all, and what conditions are necessary for its formation.

TABLE 2

	Locality	Source	Habit and Dimensions	Forms	Paragenesis	Remarks
1	Chihuahua, Mexico	U.S.N.M. #95917	Prismatic 2 mm.×.05–.1	*a,c*	Calcite and pseudomorph after unknown mineral	Flat, platy casts after—?
2	Los Lamentos, Chih., Mexico	U.S.N.M. #95897	Prismatic 1.5–2×.2–.3	*a,c*	Calcite, Descloizite	Brown Inclusions—ends clear
3	Santa Eulalia, Mexico	U.S.N.M. 4 Specimens	Prismatic 1–2×.1–1	*a, c, d, e, S, u, V*	Hematite, pseudomorph, willemite, fluorite, calcite	Cavernous limonite. Willemite coating cerussite
4	Mina da Prequiça	Harvard #1463	Prismatic 1.5×0.3	*a, m, c, e*	Limonite, cerussite	Cavernous limonite. Willemite coating cerussite
	Sobral da Adiça, Portugal	Harvard #91751	Prismatic 1×.4	*a, m, I, J, c, e S, V*	Limonite, cerussite	Willemite on limonite-coated cerussite
5	Hillsboro, N. M.	A.M.N.H. #21267	Short Prism. 2×2	*a,c,e*	Limonite, cerussite, descloizite	Crystals in cavities in massive willemite
6	Hilltop, Arizona	A.M.N.H. #21263	Prismatic 2×1	*a,c,e*	Cerussite	In cavernous igneous rocks
7	Evergreen, Colo.	A.M.N.H. #21265	Prismatic 2×1	*a,c,e*	Limonite, malachite, azurite	In cavities in fluorite

A large number of specimens from new willemite localities were examined, and they are listed in Table 2. As will be seen, the morphology of these crystals is simpler than that of the Franklin willemite. This is natural, as the conditions under which it crystallized were undoubtedly more uniform than was the case at Franklin, where the willemite shows several generations and, undoubtedly, was formed under a wide range of conditions.

In general, the crystals of these new localities are more or less elongated first order prisms, often terminated simply by the form *c*, but sometimes showing additional forms such as *e*, *u*, and *V*. A striated prism zone and *I* and *J* are not uncommon, but *m* is frequently lacking. The crystals from these localities are, without exception, small; in most instances ranging up to 2 mm. in length and half that size in diameter. Fluorescence of the supergene willemite is less marked than that of Franklin; under the quartz mercury-vapor lamp it was observed in only one specimen from Mexico (Mina Sieja) and one specimen from the west (Hilltop, Arizona). Fluorescence is reported by Spencer (1927)[1] as being observed on specimens from Rhodesia and on crystals from Lusaka.

The Mexican material was kindly loaned by the United States National Museum. One occurrence has been described by W. F. Foshag (1934). Several different localities are represented in the collection. Four specimens are from the Mina Sieja, Santa Eulalia, Chihuahua. They vary somewhat in appearance, but all four are marked by a reddish coloration caused by associated and included hematite. All are cavernous and show an earlier generation of compact botryoidal willemite with crystal surfaces, and have later growths of larger free crystals with terminations and well-developed forms. The earlier and more compact willemite tends toward redness and opacity, while the succeeding crystals are colorless and clear. There are later crystals of calcite and small cubes of fluorite on two specimens. Red hematite formed early, either contemporaneous with or preceding the willemite; the fluorite and some of the calcite is later than the last of the willemite crystals. One of these specimens of the early botryoidal willemite shows weak fluorescence under the cold-quartz lamp.

Two more specimens from the same district were studied. A specimen from the 7th level of the Ahumada Mine, Los Lamentos (USNM #95897), is a solid mass of loosely intergrown (1.5 to 2 mm. in length) deep red needles of willemite, slightly barrel-shaped with clear ends terminated by *c*, and 0.2 to 0.3 mm. in diameter. A small amount of calcite and a few small crystals of descloizite have formed after the willemite, while hematite obviously ceased forming before the end of the willemite stage.

---

[1] L. H. Bauer writes that all of his Balmat specimens, and nearly all the other "foreign" specimens, fluoresce in short ultra violet wavelengths, also under a spark gap. In any case, the broad fluorescence band of Franklin material is unlike that of any other locality.

A seventh specimen from the Berta Mine, LaCeja District of Chihuahua (USNM #95917), consists of successive crusts of white, flatly radiating willemite. These rosettes probably crystallized upon some platy mineral which has since been dissolved. At the rosette edges are some well terminated colorless crystals, 1.5 to 2 mm. long, and 0.1 to 0.5 mm. in diameter. The only mineral associated with the willemite on this specimen is some calcite which was deposited later.

Two specimens of similarly supergene willemite were obtained from the Harvard collection through the kindness of Dr. Harry Berman. These came from Portugal, the Mina de Prequiça, Sobral da Adiça. They are very different in appearance, and consist principally of limonite crusts, in the cavities of which cerussite has crystallized in fine small twins. In one of the specimens (Harvard #91751) the cerussite has been coated with a thin limonite layer, before the 1 mm. needles of willemite were deposited. These needles show a rather more complex form development than any of the Mexican specimens, *a*, *I*, *J*, and *m* were seen in the prism zone, and *c*, *e*, *V*, and *S* make up the terminations. The second specimen, on which there has been no limonite coating deposited after the cerussite, shows needles with strongly striated prism zones and less complex terminal forms.

Specimens from a few new localities in the United States were also studied, and very similar crystals were found. Two of the localities, Hillsboro, N. M., and Hilltop, Arizona, were discovered by Edwin Over who, with Arthur Montgomery, kindly contributed the specimens. J. W. Adams and R. V. Gaines furnished specimens from a third locality, the Augusta Mine, near Evergreen, Colorado.

The Hillsboro crystals, reaching 2 mm. in length and about the same in diameter, were the largest seen in this study. They are short prismatic to tabular, colorless to white, and well-developed. The specimens are vuggy masses composed of quartz and compact willemite with drusy pockets lined with willemite crystals. These are covered with later cerussite and descloizite crystals. The crystals all show the same few forms, *c*, *e* and *a*, with no indication of *m*. The more prismatic crystals show a greater tendency toward striated prism zones and short trains of reflections. Only the smallest crystals give good reflections, all of the others seem to represent sub-parallel growths and signals are confused. The cerussite, which followed the willemite, has in turn, been coated with a druse of quartz crystals. There is no iron stain on these crystals, nor on the willemite. In general, the iron seems to have oxidized and migrated further, before the willemite formation of these supergene deposits was concluded.

The Hilltop, Arizona, specimens show a vuggy fine-grained igneous rock, on which innumerable white to rose-colored prisms of willemite have crystallized. Associated with the willemite, and later in its period of formation, are small crystals of cerussite, some in minute but beautiful twins. The willemite is more prismatic but otherwise identical in its forms with that of Hillsboro; a striated prism zone all on and near *a*, with no trace of *m;* and *c* and *e* as terminal forms. A little hematite in one place on the specimen seems to have preceded the willemite. These specimens showed a weak fluorescence under the mercury-vapor light.

The last of the new localities, the Augusta Mine, near Evergreen, Colorado, shows identical crystals of about the same size and habit, but black in color. They occur in pockets in a green fluorite, the pockets are clearly the result of the solution of some other mineral. The willemite is associated with azurite, malachite, cerussite, barite, and red and brown stained earthy material. The ubiquitous *a*, *c*, and *e* are the only forms observed with *a* striated as usual.

The new occurrences and their characteristics are summarized in Table 2. We see there that from the standpoint of associated minerals, the manner of occurrence and the description of the specimens, there can be no question but that all of them are secondary and of supergene origin. Their associates are similar minerals, and possibly most significant of all, the willemite crystals resemble those of any other supergene locality.

All mineralogists are familiar with the formation of certain minerals as being characteristic of certain conditions. The frequent occurrence of wulfenite in the arid areas of the West is so generally recognized that collectors are surprised to find it at Phoenixville, Pennsylvania; or Southampton, Massachusetts. Nor does it occur in notable specimens at those localities; undue interest is attracted by the very rarity of the mineral. Willemite is normally not a showy mineral, and if it were to occur there likewise, as it well might, it may have been overlooked. Certain other minerals also belong to this generally recognized group of minerals characteristic of the alteration process in arid climates. Some are dioptase, descloizite, vanadinite, even chrysocolla, and less pronouncedly, pyromorphite, anglesite, cerussite, malachite, azurite, smithsonite, brochantite, cerargyrite, stolzite, etc., and many others of more local occurrence. It may be that there is no difference; that what we are referring to as arid climate weathering is merely deep and intense supergene alteration, resulting solely from a low standing water table and long periods of time. This does not seem to be the whole story, however, for aside from the unassailable chlorides, iodates or bromides, there are other minerals, with more common elements, which can be considered as diagnostic.

Often we do not know why dioptase forms instead of chrysocolla, why hematite forms when limonite might, or why phenakite crystallizes in place of bertrandite. Surely some special condition is responsible for the formation of that which we have come by experience to recognize as the unusual. The explanation of that condition is not easily determined, nor can a conclusive answer be given. In all probability, several factors have worked together to create willemite-forming conditions, or any one of several different conditions can result in the crystallization of dioptase instead of a solidified formless gel of chrysocolla.

A review of Table 1 shows us that in the great majority of cases willemite has formed as the result of sulphide alteration, and furthermore, that in most of those cases the climate at the locality at the present time is arid. In this table the genesis column indicates the origin ascribed by the original author, or a successor, writing about the locality, when no sign (!) follows the origin given. "Supergene!" or "hypogene!" means that no origin is given, but the description and associated minerals indicate that this is a safe assumption. A question mark indicates that the origin is uncertain. The Northern Rhodesian occurrences were originally described as being hypogene, although Spencer (1927) does not commit himself, but the appearance, associations and relationships all make the supergene origin a strong possibility. The associated minerals of the supergene occurrences are usually those which we have recognized as being typical of arid climates, or often found under similar conditions.

Having shown that willemite characteristically forms as a secondary mineral, and is only rarely and in unusual circumstances the result of hydrothermal reactions, we are confronted with the problem of what those conditions are and where we should look and expect to find additional occurrences of willemite. The primary ore is sphalerite everywhere that primary ore has been found in these willemite occurrences, and it can safely be assumed to be the original mineral elsewhere. Siliceous solutions are also necessary, and an oxidizing environment. There are a number of alternative theories which can be called upon to explain the formation of willemite. The occurrence and associations in many cases indicate that it is a mineral characteristic of secondary alteration in a region where arid climates now prevail. Utah, Mexico, New Mexico, Arizona and Portugal are all such regions. On the other hand, we have notable quantities of willemite at Morésnet and Balmat, neither locality is, at present, an arid region. Consequently, some factor which is frequently active where the climate is dry must sometimes be present elsewhere, to explain these occurrences if we assume oxidation under present climatic conditions. We have several alternatives to discuss.

In an arid region with infrequent precipitation it is natural for the oxidation process to exceed the removal of material in solution; this reaches its climax in the Atacama Desert. In moist climates the soluble sulphates are undoubtedly removed as soon as they are formed, and the concentration of salts in solution is never high. In arid climates, on the other hand, oxidation must continue between rains, and leaching take place only for a brief period as the precipitated water slowly sinks through the rocks. Consequently, concentrations must be high. It is possible that this is the controlling factor. Similar conditions of concentrated solutions could occur, due to peculiarities in water passageways, in places with humid climates, such as Balmat, Evergreen, and Morésnet. An alternative which should not be overlooked is that the alteration to willemite may have taken place under very different climatic conditions than those now prevailing. Alternative one is, then, concentrated solutions. This could also function in the hypogene deposits.

Alternative two deals with the composition of the solutions. The oxidation of the associated minerals of the primary ore may result in very different supergene solutions and some undeposited element, or group of elements, may influence the precipitated minerals. Acidity of the solutions, or lack of it, caused by an abundance or scarcity of pyrite in the original deposit, might well influence the mineral formed. Further, an originally acid solution might be more or less neutralized by solutions rich in carbonate compounds descending from overlying rocks. Alternative two has then two phases: one of relative acidity, or of actual differences in elements present. Manganese is frequently associated with willemite and is shown in many analyses; it might conceivably be a critical factor, though this does not seem probable.

Marcasite is a mineral which might be kept in mind as bearing upon both the first two alternatives. Its great ease of oxidation, together with the excess sulphur which it seems to release could be an important item in both the acidity of the solutions and the concentration due to rapid oxidation. It is not uncommon in the Joplin area, where no willemite has yet been reported; and so may have an inhibitive effect upon the formation of that mineral. In abundance it may even affect the next alternative.

Alternative three is one of temperature. Fairly high temperatures may be attained simply through oxidation in a confined space, as the writer has observed in the Missouri sink-hole iron deposits. Such an increase in temperature might easily take place under conditions of rapid oxidation with a relatively small amount of moisture and a slow circulation in a confined area. A rise in temperature might also be brought about by oxidation taking place at a considerable depth. It can readily be seen that in neither case would there be a very high temperature, but we have no way of knowing what the critical point is between the formation of hemimorphite and willemite. It may be at a comparatively low temperature.

Another factor which may work in conjunction with those above, or alone, is that of pressure. Oxidation taking place at the depth of the water table in arid regions may well be under considerably more pressure than oxidation taking place only a few feet below the surface. This may not be of significance, for spaces which are not filled with water to the surface should be under little greater pressure than similar open spaces at the surface. Water-filled rocks, however, at depths of one or two thousand feet should be under considerably higher pressures and the reactions would take place under conditions different from those prevailing near the surface. It would be logical to expect different products.

The hematite-limonite relationship is closest to the willemite-hemimorphite parallel and it is undoubtedly of significance in any interpretation. It has been suggested that the explanation which may be valid for Franklin (formation of willemite from the metamorphism of hemimorphite), will also hold for other localities and that a dehydration of supergene ores through mild metamorphism is universally responsible. There is said to be evidence of such dehydration of weathered products at Hillsboro, Tres Hermanas, and Beaver County, in addition to Balmat, and it may be asked, why, if arid climate weathering alone is responsible, are there not still more frequent occurrences of willemite. In this case the function of the arid climate is merely that of providing a low water table, permitting deeper supergene alteration than prevails in more humid regions. Postoxidation igneous activity is not marked at most of these new localities. Lindgren (1905) and Foshag (1934), for instance, both speak of the oxidation as if it post-dated any igneous emanations, though their failure to mention it does not, of course, mean that there is none. The authorities describing the regions may have considered such hypogene solutions unimportant, as they would be from a standpoint of ore introduction.

There are doubtless other factors which may be involved, and certainly the problem is not a simple one. Willemite is frequently made synthetically. Morey and Ingerson (1937) list several successes, and it is now being made for the new fluorescent lights by the General Electric Company, but the methods all involve relatively high temperatures. These successes in synthesis thus in no way contribute to the problem of its slow formation in nature at low temperatures. A few facts about the occurrences stand out which are of interest, worthy of note, and possibly of value in a final interpretation.

Willemite formed under conditions of secondary alteration is uniform in size and crystal habit, in its paragenesis, its distribution and its appearance. This would indicate its formation under essentially similar conditions. We know that it can also form under abnormal conditions of high temperature from hypogene solutions. Then it varies in those qualities previously listed for supergene willemite. Hematite is a more frequent associate of willemite, limonite more common with hemimorphite. These facts we know, the rest we shall have to work out.

Of all of the alternatives proposed, the writer believes that the most important is that of concentration of solutions. Willemite may be the characteristic precipitate from saturated solutions, hemimorphite the product of weak solutions. Undoubtedly, other factors play their part, but in all the phenomena of mineral formation in arid climates we find one thing, a local concentration of elements usually widely disseminated in small quantities. Wulfenite and vanadinite, cerargyrite and descloizite are typical of arid regions and of this statement. All represent a local congestion of normally disseminated elements and it is not improbable that willemite, their frequent associate, is another manifestation of the same processes.

The alternative suggestion is well worth considering, though we still have the problem of the cause of the mild metamorphism. If it is correct, we may expect to find additional occurrences of willemite where extensive pre-Cambrian oxidation of zinc sulphide has been preserved and later metamorphosed, or in regions near centers of volcanic activity in more recent times, giving rise to local metamorphism of the secondary products of oxidation.

But the problem is not a simple one which can be solved by rationalizing at a desk or in a laboratory. Let us examine more occurrences in greater detail and let us learn more about why hematite forms; let us examine zinc deposits, especially in dry climates with our eyes open, and we may find the inconspicuous, but interesting willemite. When we have done that, we may gain a conception, not only of the processes by which willemite forms, but also of the entire problem of supergene alteration and secondary mineral formation. Then, too, we can think about wulfenite and dioptase, vanadinite and brochantite, gems of the collectors' cabinet but still mysteries to the mineralogist.

BIBLIOGRAPHY

Boggild, O. B., *Mineralogia Groenlandica, Med. om Grønland*, **32,** 276–278 (1905).

Brown, J. S., Supergene sphalerite, galena and willemite at Balmat, New York: *Ec. Geol.*, **31,** 331–354 (1936).

Buttgenbach, H., *Abs; Min. Abs.*, **3,** 351 (1927).

Clark, R. W., A new occurrence of crystallized willemite: *Am. Mineral.*, **1,** 89–91 (1916).

Foshag, W. F., The ore deposits of Los Lamentos, Chihuahua, Mexico: *Ec. Geol.*, **29,** 330–345 (1934).

Genth, F. A., Contributions to mineralogy: *Proc. Am. Phil. Soc.*, **24,** 43 (1887).

Lacroix, A., *Min. de France* **4,** 719–721 (1910); *Min. de France* **5,** 84 (1913).

Lindgren, W., and Hillebrand, W. F., Minerals from the Clifton-Morenci District, Arizona: *Am. Jour. Sci.*, (IV), **18,** 448–460 (1904).

Lindgren, W., The copper deposits of the C.-M. District, Arizona: *U.S.G.S. Prof. Paper*, **43,** (1905).

Lindgren, W., *Mineral Deposits* (1919).

Morey, G. W., and Ingerson, E., The pneumatolytic and hydrothermal alteration and synthesis of silicates: *Ec. Geol., Supp. to*, **32,** 607–761 (1937).

Palache, C., Mineral notes on Franklin and Sterling Hill, N. J.: *Am. Mineral.*, **13,** 326–329 (1928).

Palache, C., The minerals of Franklin and Sterling Hill, Sussex Co., N. J.: *U.S.G.S. Prof. Paper*, **180,** 82–88 (1935).

Palache, C., and Graham, R. P. D., On the crystallography of willemite: *Am. Jour. Sci.*, (IV), **36,** 639–644 (1913).

Penfield, S. L., Contributions to the crystallization of willemite: *Am. Jour. Sci.*, (III), **47,** 305–309 (1894).

Spencer, L. J., South African occurrences of willemite: *Min. Mag.*, **21,** 388–396 (1927)

LINEAR THERMAL EXPANSION AND INVERSIONS OF QUARTZ, var. ROCK CRYSTAL

Joseph L. Rosenholtz and Dudley T. Smith,
Rensselaer Polytechnic Institute, Troy, New York.

Abstract

A new apparatus is described for the measurement of linear thermal expansion between 0° and 1000° C. and for the determination of inversion points. Results are given for expansion of Brazilian rock crystal perpendicular and parallel to the principal axis. The α-β inversion was found at 573.1±0.5° C. A second change was observed at 872±1° C. for sections cut perpendicular to the principal axis. This change, ascribed to the quartz-tridymite inversion, was observed on only one of four parallel sections. The remaining three showed a sudden acceleration in the rate of contraction at 830±2° C.

Introduction

This is the first of a series of experimental studies of the linear thermal expansion of crystallographically oriented sections of rock-forming minerals at temperatures from 0° to 1000° C. The lack of such information, except for relatively few minerals, and its potential usefulness in geophysical studies has prompted this extended program. Despite the fact that reliable data is available for quartz, this mineral was selected because it would serve to test the accuracy of the special equipment devised for the expansion and inversion measurements herein described.

Description of Apparatus

The new apparatus is, in effect, a combination of a Chevenard type of differential dilatometer and a specially constructed capillary cell, a vertical section of which is shown in Fig. 1. The three principal parts are the capillary cell *A*, the advancing mechanism *B*, and the connecting block *C*, which also holds other measuring attachments. Except as will be indicated, all parts were machined from cold rolled steel. A circular recess *P* was turned in the front of the block. A circular, aluminum gasket *W* fits snugly into the face of *A* at the edge of this recess. The diaphragm *X*, made of 0.0035 in. shim steel, is held against the gasket by the restraining plate *N*. This plate is fastened to *A* by a series of closely-spaced bolts and is bored to receive the nut on the screw of part *O*. In order that the motion of expansion may be imparted to the diaphragm without twist, the bolt *O* has an extension which slides smoothly in *R*. The latter has several radial holes drilled through from the center to allow the mercury which fills the cell to flow freely without compression. The screw end of the bolt is cut to a sharp 90° cone to receive the ground point of the fused quartz rod *G*.

Two vertical holes are drilled into the cell block, one of them being shown at *S*. When pressure is applied to the diaphragm, mercury flows through *S* to the capillary tube. The latter is fastened to the cell by the collar *T* into which it is cemented. Tubing of various capillary bores may be used to register the displacement of mercury in the cell. For the range of displacement experienced during the expansion of quartz, it was found that a bore of 0.75 mm. gave excellent results. Regardless of bore size, it is important that the tubing be carefully selected for uniformity. The tube extends about one meter in a direction away from the reader. A Beckmann differential thermometer is cemented into the second hole (not shown in Fig. 1) with the bulb totally immersed in the mercury. The cell is filled through the glass stopcock *Z* which was specially ground to insure against leakage.

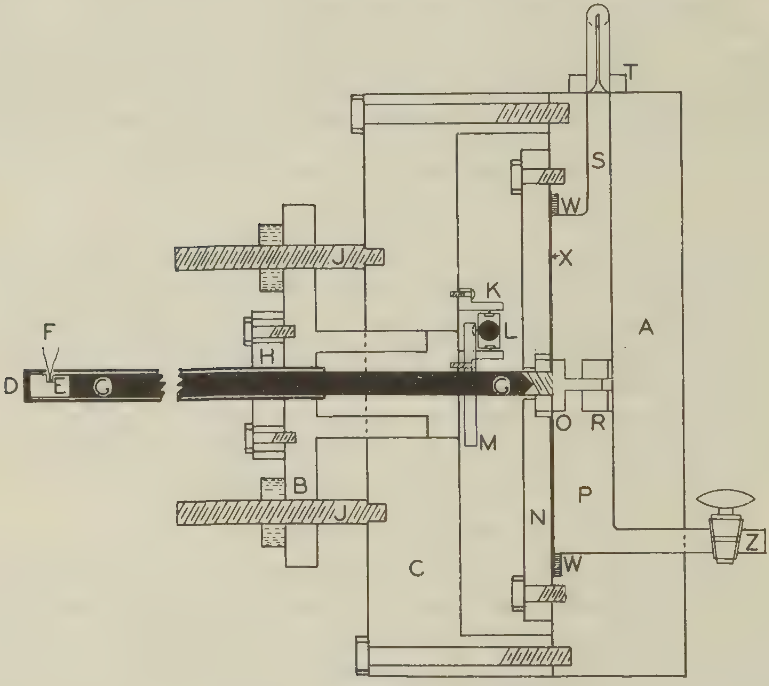

FIG. 1. Vertical section of capillary cell apparatus.

The advancing mechanism *B* holds the fused quartz tube *D*, the sample *E*, and the fused quartz rod *G*. The end of the tube was closed by fusing on a flat. All fused quartz is transparent vitreosil. The inside end of the tube and the corresponding end of the rod are ground flat. A thermocouple *F* is made from *B.* & *S.* No. 30 platinum and platinum-10% rhodium wires obtained from Baker and Company. This is brought through a hole drilled in D into the depression drilled in the sample. The thermocouple was frequently calibrated against similar thermoelements certified by the Bureau of Standards. The tube is cemented into the plate H which is bolted to B in such a manner that its orientation may be varied in order to center G with respect to the cone in O. The entire unit B is advanced toward the diaphragm on the fine-threaded studs J. Block C is bolted to A so that a rigid unit is obtained.

A circular ring M, cemented to G, imparts the advance motion to the lever mechanism K. The lever rod L is made of fused quartz and is mounted in jewel bearings. The end of the lever opposite from the reader makes contact with an Ames indicator which is rigidly attached to C. This indicator has ten-thousandth inch divisions and was made with a friction of only 5 grams. Its sensitivity is 0.00001″ and it is precise to less than ±0.000025″.

The complete cell assembly and projecting capillary tube are enclosed in a large air bath built of double-walled celotex. The air temperature is controlled by a mercury thermoregulator and relay and the air circulation is maintained by a blower which is separately and externally supported. Vibration is eliminated by a sheet of Foam Sponge rubber under the air bath. The fused quartz tube projects through the front wall of the bath and a tubular electric furnace slides over it to a predetermined position such that the hot junction of the thermocouple is at the hot spot of the furnace. This arrangement insures a uniform temperature over the length of the quartz sample.

Movement of the mercury in the capillary tube is observed through a double-walled plate glass window and is measured by a horizontal cathetometer which reads to 0.02 mm. Temperatures are measured with a Leeds & Northrup Type K_2 potentiometer and Weston cell.

It seems advisable at this point to explain the necessity for certain parts of the cell apparatus. The restraining plate prevents the diaphragm from bulging and also permits its restoration to approximately the same point. If absolute restoration were possible—and such was not found to be the case—direct calibration of a particular diaphragm and capillary tube could be accomplished. The minute variations in diaphragm restoration from one determination to the next is a possible source of error. Many trials established that this error was too great to permit reliable values to be obtained. While the variations would be of minor consequence where reasonably large movements (over 0.05 mm.) were involved, the expansion of a 10 mm. parallel section for a temperature interval of 25° is only approximately 0.002 mm. It was concluded, therefore, that the most certain method should include a calibration to be obtained coincidentally with the expansion of each test section. The lever and indicator arrangement makes this a possibility. Their calibration was obtained interferometrically. An obvious question is, "Why not use the indicator and lever alone and eliminate the complications of the capillary cell?" The answer is that, for small expansions, such as the amounts obtained up to a few hundred degrees, the indicator and lever arrangement alone is not adequate. Higher indicator values can be used with full confidence and these, in conjunction with the cathetometer readings, permit the true values for small expansions to be computed.

PREPARATION OF TEST SPECIMENS

The sample selected was clear rock crystal from Minas Geraes, Brazil. Its density was $d_{20}=2.649$. Polished plates were used for the determination of refractive indices on an Abbe refractometer using sodium light, the results being $\omega=1.544_4$ and $\epsilon=1.553_2$. By means of a diamond saw, plates approximately 4 mm. thick were cut parallel and perpendicular to the principal axis. These plates were then cut into prisms 4 mm. square and 10 mm. long. They will be referred to hereafter as sections rather than prisms in order to avoid confusion with the crystallographic nomenclature. It would have been possible to cut sections much longer than 10 mm. This was not done because it was desired to develop a technique which would apply to minerals from which long sections could not be obtained. The ends of each section were ground flat and a small depression for the thermocouple was drilled in the center of one face. Optical examination showed that some of the plates as cut deviated slightly from the desired orientations. A special grinding machine was constructed to correct these deviations by modifying a transit theodolite to hold the quartz plates. The transit is mounted on a lathe compound so that a plate may be brought up to an FF carborundum wheel mounted on the shaft of a high speed motor. The horizontal and vertical circles of the transit permit a freedom of adjustment which corresponds to that obtained on a two-circle goniometer.

TECHNIQUE

A prepared quartz section, the length of which is measured with a micrometer caliper, is placed in the fused quartz tube, the rod is inserted, and the advancing mechanism is adjusted until the mercury in the capillary tube begins to move. The thermocouple is then connected to the potentiometer through a 0° C. cold junction, and the hot junction is inserted into the depression in the sample. It is important that the couple wires be cemented into the tube in order to avoid temperature irregularities. The air bath is maintained above room temperature and the temperature within the cell is measured on the Beckmann thermometer.

Because of the large mass of steel and the large air volume, the temperature variation within the cell is not greater than 0.1° C. during the course of a complete determination. Even so small an amount is important and corrections must be applied for any variations.

In order to obtain expansion data beginning at 0° C., rather than at room temperature, the furnace tube is packed with granules of solid carbon dioxide and is allowed to remain so for one-half hour. The furnace is then emptied and is slid in place over the fused quartz tube as explained previously. Both ends of the furnace are then packed with asbestos. By this procedure the quartz sample is chilled much below 0° C. and, because of the furnace insulation, it warms quite slowly. As soon as 0° C. is reached, readings are begun and are continued at regular intervals up to 1000° C. Readings are taken on the potentiometer, cathetometer, Ames indicator, and Beckmann thermometer. Furnace temperatures are controlled by a Variac adjustable transformer which has been calibrated, thus making it possible to regulate the rate of heating very closely. All determinations were made only during heating and the rate was such that no sections were cracked when finally cooled to room temperature.

Results

We shall first consider the results obtained with sections cut perpendicular to the *c*-axis. Since there is a distinct difference in piezoelectric properties in equatorial sections cut parallel to the first and second order crystallographic directions, it was thought that a variation might be found in their linear thermal expansions. As a consequence, three sections were studied for each of these equatorial orientations. Because all results were found to be the same, within the range of experimental error, they were cast as a single equatorial mean, the values being given in Table 1. The last column lists the most probable values for the perpendicular orientation as presented by Sosman.[1] His data is the result of a most careful analysis of all previously published work on quartz and is more reliable for comparison than the results of any individual investigator. With the exception of the coefficients at 573° and 1000°, there is a remarkably good agreement. Since there is a large personal element involved in determining when the rate of expansion changes at the inversion point, it is easily conceivable that a substantial difference might occur here. It should be said, however, that it is not difficult to observe the change with the equipment described, and that the α-β change is very sharply defined. Sosman's data above 573° is not derived from many linear determinations, as contrasted with numerous values in the lower temperature range. Still another consideration is the variation which is found in different quartz samples.

[1] Sosman, R. B., *The Properties of Silica* (**1927,** New York), p. 370.

Four sections were studied in the direction parallel to the principal axis. The results are given in Table 2, together with Sosman's[2] corresponding values. A comparison of both columns reveals a close agreement up to 500° but divergence above that temperature, except where the inversion begins. It is to be noted that in both orientations the maximum observed values are lower than those previously reported.

TABLE 1. EQUATORIAL MEAN COEFFICIENT OF LINEAR THERMAL EXPANSION FOR QUARTZ.

0° C. to		R. & S. $10^6\delta_m\perp$	Sosman $10^6\delta_m\perp$
100°		14.37	14.45
200°		15.62	15.61
300°		16.81	16.89
400°		18.37	18.50
500°		21.04	20.91
550°		23.58	23.40
573°	Before	26.17	25.15
	After	30.48	31.02
600°		29.53	29.71
700°		25.22	
800°		22.18	22.18
900°		19.64	
1000°		17.69	16.97

TABLE 2. AXIAL MEAN COEFFICIENT OF LINEAR THERMAL EXPANSION FOR QUARTZ.

0° C. to		R. & S. $10^6\delta_m\|$	Sosman $10^6\delta_m\|$
100°		7.82	7.97
200°		8.64	8.75
300°		9.52	9.60
400°		10.53	10.65
500°		12.02	12.22
550°		13.43	13.81
573°	Before	15.00	15.00
	After	17.03	17.98
600°		16.60	17.08
700°		14.15	
800°		12.41	12.02
900°		10.88	
1000°		9.45	8.83

---

[2] *Ibid.*

The critical point for the α-β inversion was determined on 14 different specimens, all cut from the same crystal, and was found at 573.1 ± 0.5° C. This is in excellent agreement with the very carefully determined values of Bates and Phelps[3] who reported the limits 573.2° and 573.4° C.

A second change was found in all perpendicular sections at 872 ± 1° C. The change was observed simultaneously on the mercury cell and the indicator as an abrupt, though small, increase in the rate of contraction. The amount of contraction at this point is approximately 0.1 per cent. If this is contrasted with the large expansion at 573°, it is obvious that there is no appreciable difference in the value of the mean coefficient at 872° before and after the change. It appears most likely that this represents the quartz-tridymite inversion which was reported at 870 ± 10° C. by Fenner.[4] This change was observed at 871.5° for only one of the four parallel sections. The remaining three showed a marked acceleration in the previous uniform rate of contraction at 828.2°, 831° and 830°, the mean being 830 ± 2°. It is possible that, due to this acceleration, the 872° point was obscured. Since the quartz-tridymite inversion is extremely sluggish in the temperature range where the change was observed, except in the presence of fluxes and no fluxes were used in this work—no apparent explanation is at hand for the uniformity of perpendicular sections and the lack of uniformity of the others.

SUMMARY

The results of this research indicate the validity of the new apparatus as an instrument for the precise determination of both linear thermal expansion and inversion points. Since the source of the quartz used by previous investigators is not reported, an exact comparison with their work is impossible. It is to be noted that the quartz-tridymite inversion had not been observed previously in any similar investigations.

ACKNOWLEDGMENTS

It is with deep appreciation that the authors express their gratitude to the Carnegie Corporation of New York, whose grant-in-aid made it possible to obtain the precision instruments for measurement and calibration which were necessary for this research program. They are indebted to W. & L. E. Gurley, Troy, New York, for their cooperation in the development of the transit grinding equipment. It is also a pleasure to acknowledge the helpfulness of Professors George Howard Carragan and Harold A. Wilson of the Rensselaer Polytechnic Institute.

---

[3] Bates, F., and Phelps, F. P., The new fixed point on the thermometric scale: *Physical Rev.* (2) **18,** 115–116 (1921).

[4] Fenner, C. N., The stability relations of the silica minerals: *Am. Journ. Sci.*, **36,** 331–384 (1913).

COLORADO CERITE

Ross A. Hanson* and D. W. Pearce, *Dept. of Chemistry, Purdue University, W. Lafayette, Indiana.*

Abstract

Chemical analyses of samples of cerite from near Boulder, Colorado, give evidence for the formula $2CaO \cdot Al_2O_3 \cdot R.E._2O_3 \cdot 2SiO_2$ with a considerably higher Al_2O_3 content than heretofore observed in other samples. Some discussion is given concerning the peculiar structural relations existing between the purple fluorite (enclosed in the cerite and concentrated centrally), the cerite itself and its surrounding narrow border of black allanite. Combined spectrographic and chemical determination of the individual rare earths in the cerite and allanite shows that these minerals fit into their prescribed type in the Goldschmidt-Thomassen classification.

Introduction

The recent article by E. N. Goddard and J. J. Glass[1] has thoroughly described the interesting radioactive cerite which occurs near Jamestown, Colorado. This cerite had been called to the attention of the present writers by Mr. Jack Ingram of Boulder, Colorado, and was considered first as a possible source of rare earth group material for chemical work.

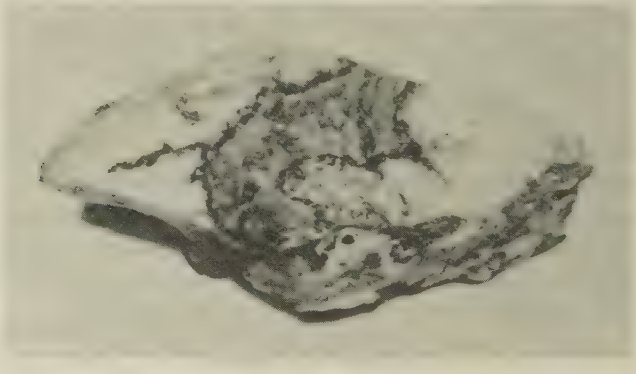

Fig. 1. Gray cerite with black border of allanite enclosed in sugary quartz. × $\frac{3}{4}$.

Aside from the fact that this was the first discovered occurrence of cerite in the United States, two observations on the sample first acquired

---

* Part of a thesis to be presented by Ross A. Hanson to the Graduate School of Purdue University in partial fulfillment of the requirements for the degree of Master of Science in Chemistry.

The authors wish to express their gratitude to the Purdue Research Foundation which has sponsored this and other work upon the geochemistry of the rare earth elements.

[1] *Am. Mineral.*, **25**, 381–404 (1940).

(Fig. 1) suggested some further study of the mineral. The first and most outstanding point observed was the thin, sharp shell of black material completely encircling the gray cerite lens and, in one place, running in a narrow stringer out into the surrounding sugary quartz. Qualitative examination showed that this "black border" was also a rare earth mineral. As it appeared probable that the two minerals had crystallized practically simultaneously from the same pegmatite liquor their close association seemed to offer an unusual opportunity to study the distribution of the individual rare earths between two such phases.

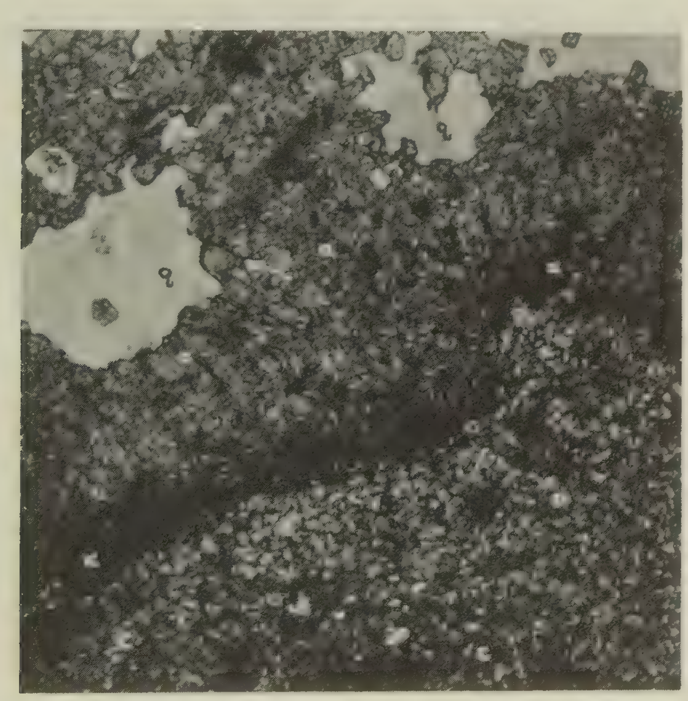

FIG. 2. Cerite (*c*)—allanite (*a*) contact, showing unidentified mineral (*x*) and quartz (*q*) inclusions in the allanite. ×32.

In the second place, close examination of the cerite itself, even with the naked eye, revealed the presence of minute specks of an unknown purple material concentrated in the central part of the mass. This material possessed the characteristic color of neodymium salts and further heightened the interest in this unusual mineral assemblage.

With the hope that some further discussion of these rare minerals might be of interest, our microscopic observations, chemical and spectrographic analyses and deductions therefrom are here presented.

Thin-Section Examination

Examination of several thin sections prepared from various specimens revealed interesting features. The "black border mineral" is yellow-brown in thin section (Fig. 2) and short crystals of it project at the contact into the surrounding (rarely enclosed) quartz and feldspar. The sharp terminal faces against the gangue minerals give good evidence of its earlier crystallization. Goddard and Glass have identified this mineral as allanite by its optical properties as well as by its chemical composition. The allanite is not homogeneous throughout but contains a considerable amount of an unidentified black material which is highly concentrated in the form of specks and masses at the allanite-cerite border (Fig. 2). It appears to be entirely within the former as it presents a fairly sharp contact with the cerite, but becomes scattered and spread out away from this contact and toward the central part of the allanite band.

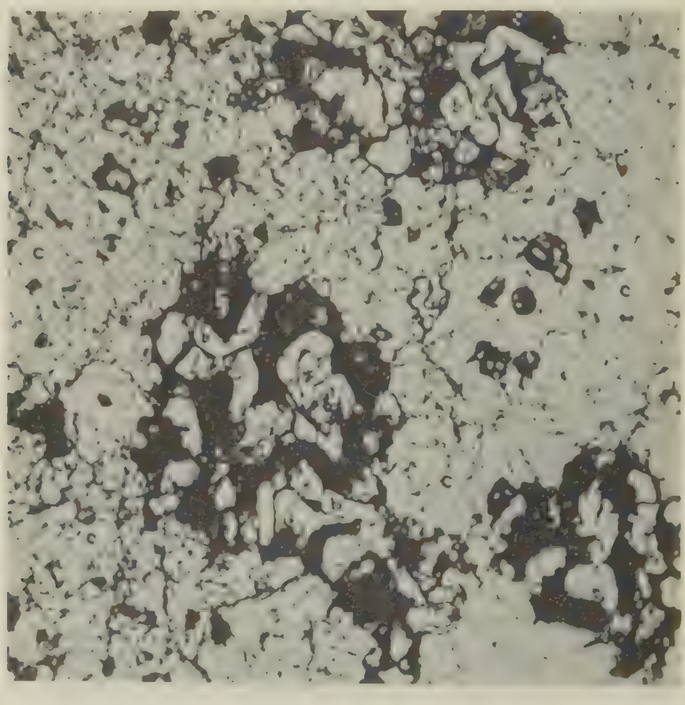

Fig. 3. Purple fluorite (*f*) in gray cerite (*c*). In places the fluorite has broken away leaving balsam (*b*). ×125.

The cerite itself is gray and is made up of variously oriented grains showing no crystal faces but interlocked to present a texture approaching a mosaic. The enclosed purple material has been identified by Goddard and Glass as fluorite. It occurs in the form of irregularly shaped masses which, in the central part of any particular cerite lens, become gathered into rosette-like groups roughly circular in shape (Fig. 3). Toward the boundaries of the cerite the rosettes become fewer and smaller and the purple segregations themselves very much more scattered until, close to the border, they are absent altogether.

The complete interpretation of the textural features of this intergrowth of minerals is not immediately clear. The allanite may have been rejected by the cerite as the latter crystallized and hence forced to the periphery where it crystallized with regular contact against the cerite while its crystals grew out into the remaining unsolidified pegmatite liquor. This hypothesis, however, is difficult to rationalize with the concentration of the purple material in the central parts of the cerite lenses. The irregularity in outline of this purple material would seem to require that it was segregated from the cerite melt and remained liquid after the solidification of its host material. Such segregation and concentration centrally would suggest, however, that the cerite masses cooled more rapidly at the borders than in the interior and therefore would seem to contradict the above suggested mechanism for the rejection of the allanite to the borders.

The opinion of Goddard and Glass that the allanite forms "replacement borders" (p. 386) would require the influx of younger pegmatite liquors after, or during, the solidification of the first and might be expected not to result in the fairly sharp contacts with the cerite, such as are to be observed in all our samples. Furthermore, spectrographic investigation has shown that the content of individual rare earths is much the same in the two minerals. Such similarity in the original and the replacing solution would seem unlikely.

Chemical Analysis

In Table 1 is given the data resulting from the chemical analysis of the cerite and of its black border, allanite. The results are here compared with those of Goddard and Glass.

TABLE 1. ANALYSES OF CERITE AND ASSOCIATED ALLANITE

	‘Cerite Rock”		Pure Cerite Calc.		Allanite	
	G. & G.	H. & P.	G. & G.	H. & P.	G. & G.	H. & P.
SiO_2	18.78	16.71[a]	18.10	17.42	30.40	37.73
$Al_2O_3(TiO_2)$	0.24	14.00	0.32	14.59	10.25	17.07
FeO	1.17	1.34	1.54	1.40	10.29	5.69
Fe_2O_3	—	—	—	—	10.33	0.80[b]
U_3O_8	0.51	spect. tr.	—	—	—	spect. tr.
Ce_2O_3	28.85	20.77[c]	32.97	21.65	14.61	7.39[d]
$(La, Tb)_2O_3$ etc.	27.20	26.43	35.72	27.55	10.32	17.54
Y_2O_3 etc.	2.94		3.86			
ThO_2	0.28	none	—	—	—	none
MnO	0.17	0.38	0.22	0.40	0.66	0.78
ZnO	none	none	—	—	—	spect. tr.
CaO	12.55	16.55	5.80	15.24	7.47	7.56
MgO	0.16	1.61	0.21	1.68	1.44	3.44
PbO	0.07	spect. tr.	—	—	—	spect. tr.?
Na_2O	—	—	—	—	0.02	s[e]
K_2O	—	—	—	—	0.16	tr.
TiO_2	—	none	—	—	1.46	s[e]
H_2O	0.96	0.067	1.26	0.07	1.95	0.145
CO_2	1.00	none	—	—	—	none
P_2O_5	none	—	—	—	—	—
F	5.94	1.30[f]	—	—	—	0.01
Cl	none	—	—	—	—	—
B_2O_3, BeO	none	none	—	—	none	—
	100.82	99.16	100.00	100.00	99.36	98.16
Less O for F	2.52	0.55				0.00
	98.30	98.61			99.36	98.16

[a] Includes 1.02% SiO_2 calcd. lost as SiF_4 during dissolution of the sample.

[b] Sample was finely chipped in removing from cerite and all Fe $^{+3}$ may have come from Fe^{+2}.

[c] By spectrographic method av. 23.16% (see Table 3).

[d] By spectrographic method av. 8.88% (see Table 3).

[e] Detected by spectrograph.

[f] Used as correction for SiO_2 see (a).

Cerite

The recalculated analysis of the cerite gives the following molecular ratios:

	G. & G.[a]	H. & P.
SiO_2	301	290
TiO_2	—	—
Al_2O_3	3	143
Fe_2O_3	—	—
Ce_2O_3	100	148[c]
RE_2O_3	125[b]	
FeO	21	19
MnO	3	6
CaO	103	272
MgO	5	42
Na_2O	—	—
K_2O	—	—
H_2O	70	4

[a] Calculated from the data presented by Goddard and Glass.

[b] Molecular weight of $R.E._2O_3$ taken as 331.

[c] Molecular weight calculated from combined chemical and spectrographic data 331.37.

When compared with the cerite analysis as announced by Goddard and Glass and the corresponding molecular ratios, the new results reported above present several points of interest. Notable first is the great contrast in the amount of Al_2O_3 present; as pointed out by the previous investigators, the per cent of this constituent has not previously been found higher than 2.64 in all the published analyses of this rare mineral. Outstanding also is the very low, almost insignificant, H_2O content; this, however, is in very good accord with the fresh appearance and apparently unaltered nature of all the material which we have obtained from this source. The molecular ratios calculated from these results are coherent: the formula appears quite definitely to be $2\ CaO \cdot Al_2O_3 \cdot R.E._2O_3 \cdot 2SiO_2$. It is felt that Al and Rare Earths should not here be regarded as vicarious constituents; in the first place it would require a fortuitous circumstance that the ratio of $Al_2O_3 : R.E._2O_3$ be 1:1 as it is here, and in the second place the ionic sizes of Al^{+3} and $R.E.^{+3}$ are greatly different.[2] It would seem more probable, as indeed it is assumed by some for many other minerals, that $R.E.^{+3}$ and Ca^{+2} are replaceable the one by the other within limits.[3] It must also be pointed out that the significance of the monoxides is not clear; in neither the results of Goddard and Glass nor in those here reported may the molecules of other divalent elements be added to the CaO without rather badly disrupting an apparently excellent fit. It may later be found to be of significance that in both analyses the sum (2H,

---

[2] Goldschmidt, V. M., *Geochemie, Handworterbuch d. Naturwiss., Zweite Aufl., Bd.* **2,** 886–904 (1933); *Kristallchemie, ibid., B.* **5,** 1–27 (1934); Principles of distribution of chemical elements in minerals and rocks: *Jour. Chem. Soc.*, 655–673 (1937).

[3] Goddard and Glass (*ibid.*, p. 596) have briefly considered this possibility.

Fe, Mn, Mg)O is in a simple ratio to the chosen unit; thus in the earlier work this ratio is 99:ca 100 (or 1:1), whereas in the present work it is 71:ca 142 (or 1:2).

The cerite analysis reported by Goddard and Glass yielded the formula $CaO \cdot 2R_2O_3 \cdot 3SiO_2 \cdot H_2O$; in their ratios H_2O is low and R_2O_3 is somewhat high. The present work would, indeed, suggest that even *one* H_2O is not an essential constituent of the mineral. It does not appear, however, that the present formula could be fitted into the series tentatively suggested by Goddard and Glass even if the H_2O is regarded as unessential:

CaO-free cerite	$2\ R_2O_3 \cdot 3\ SiO_2$
Colorado cerite (G. & G.)	$CaO \cdot 2\ R_2O_3 \cdot 3\ SiO_2$
Lessingite	$2\ CaO \cdot 2\ R_2O_3 \cdot 3\ SiO_2$
Colorado cerite (H. & P.)	$3\ CaO \cdot 1\ 1/2\ R.E._2O_3 \cdot 1\ 1/2\ Al_2O_3 \cdot 3\ SiO_2$

Allanite

The molecular and atomic ratios calculated from our allanite analysis and those obtained by Goddard and Glass are as follows:

	Molecular Ratios		Atomic Ratios			
	G. & G.	H. & P.		G. & G.	H. & P.	
SiO_2	506	628	Si	506	628	Z=628=3×209
Al_2O_3	100	167	Al	201	335	
Fe_2O_3	65	5	Fe‴	129	10	
FeO	143	79	Fe″	143	79	Y=509=3×170
MgO	36	85	Mg	36	85	
TiO_2	18	—	Ti	18	—	
K_2O	2	—	K	4		
Na_2O	0	—	Na		—	
CaO	133	135	Ca	133		
MnO	9	11	Mn	9	135	X=296=2×148
Ce_2O_3	45[a]	75[b]	Ce	89	11	
$R.E._2O_3$	31		R.E.	63	150	
H_2O	108	8	(OH)	216	16	2325=13×179
			O	2095	2309	

[a] Molecular weight of $R.E._2O_3$ taken as 330.

[b] Molecular weight calculated from combined chemical and spectrographic data 331.34.

Machatschki's formula $= X_2Y_3Z_3(O, OH, F)_{13}$.

Determined by Goddard and Glass $= X_{1.79}Y_{3.17}Z_{3.04}(O, OH)_{13.88}$.

Determined by Hanson and Pearce $= X_{1.65}Y_{2.84}Z_{3.50}(O, OH)_{12.98}$.

The data require little discussion. The ratios fit the formula of Machatschki[4] probably not quite as well as do those of Goddard and Glass. The per cent of SiO_2 in the analysis is undoubtedly high. This may be due to the fact that quartz is occasionally to be found enclosed in the allanite border and also that it is difficult to manually separate the latter from the quartz in contact with it—preliminary to the analysis.

RADIOACTIVITY

Five days exposure of a polished surface to a photographic plate gave only a slight indication of radioactivity and this appeared not to be concentrated in any particular areas of the sample, but to be generally distributed throughout it, in the cerite as well as in the allanite border. There was obtained no indication that the minute particles of black mineral in the allanite were more radioactive than any other part of our samples; it cannot be assumed that they are uraninite.

SPECTRUM EXAMINATION

The intense purple-violet color of the fluorite would suggest that it carried a high content of either neodymium or trivalent manganese. Ex-

TABLE 2. SPECTROGRAPHIC ANALYSIS OF COLORADO CERITE AND ALLANITE FOR THE RARE EARTH ELEMENTS

	% R.E. metal in $R.E._2O_3+CeO_2$	
	Cerite	Allanite
Sc	abs. 100″ exp.	abs. 100″ exp.
Yt	tr.	abs. 100″ exp.
La	21 ± 3	29 ± 3
Ce	41 ± 5[a]	30 ± 3[b]
Pr	1	tr.-s
Nd	26 ± 3	30 ± 3
Sm	6.5 ± 2	5 ± 2
Eu	tr.	abs. 50″ exp.
Gd	tr.	abs. 100″ exp.
Tb	tr.?	abs. 100″ exp.
Dy	abs. 100″ exp.	abs. 100″ exp.
Ho	tr.	abs. 100″ exp.
Er	abs. 100″ exp.	abs. 100″ exp.
Tm	abs. 100″ exp.	abs. 100″ exp.
Yb	abs. 100″ exp.	abs. 100″ exp.
Lu	tr.	abs. 100″ exp.

[a] 45.2% by chemical determination and calculation.

[b] 30.64% by chemical determination and calculation.

---

[4] Machatschki, F., *Centralbl. Mineral., Geol., u. Pal.*, Abt. A, 89-96; 154-158 (1930).

amination of the mineral in thin section by means of a Leitz microspectroscope, however, revealed none of the characteristic rare earth absorption bands. On the other hand, neither were such bands detectable in the cerite or in the allanite in spite of the high content of neodymium later found to be present in both of these. The coloring matter of the fluorite is as yet undetermined.

The individual rare earths in the oxide mixture from each mineral were determined spectrographically by the use of the line density method. A Baird Associates grating spectrograph and Eastman No. 40 8″×10″ spectrographic plates were used in this work. Exposures of thirty seconds were ordinarily employed; elements were recorded as absent if no lines were to be found on greatly over-exposed plates. The data are shown in Table 2.

Table 3. Rare Earth Oxide Ratios in Cerite and Allanite

Oxide	A Ave. % in Mineral		B % in Mineral Calc. from A to chem. RE_2O_3 total		C Calc. from B to 100% RE_2O_3 $+Ce_2O_3$		Ratio to Sm_2O_3	
	Cerite	Allanite	Cerite	Allanite	Cerite	Allanite	Cerite	Allanite
La_2O_3	11.86 spect.	8.60	10.41	7.98	22.06	32.01	3.26	5.86
Pr_2O_3	pres. spect.	tr.	—	—	—	—	—	—
Nd_2O_3	14.61 spect.	8.84	12.83	8.20	27.18	32.89	4.02	6.02
Sm_2O_3	3.63 spect.	1.46	3.19	1.36	6.76	5.46	1.0	1.0
Total RE_2O_3	30.10 spect.	18.90	26.43	17.54				
Ce_2O_3	(23.61 spect.	8.88)	20.77 chem.	7.39	44.00	29.64	6.50	5.43
CeO_2	21.78 chem.	7.75	(21.78 chem.	7.75)				
$RE_2O_3+CeO_2$	48.21 chem.	25.29						
RE_2O_3	26.43	17.54						
$RE_2O_3+Ce_2O_3$			47.20	24.93	100.00	100.00		

It was felt that the chemical data for the determination of cerium was of much greater reliability than that obtained by the spectrographic method, and furthermore that the total rare earth oxide content determined chemically was more reliable than the sum of the averages of the individual oxides obtained by calculation from the spectrographic data. Consequently the total: (spectrographic) sesquioxide content plus (chemical) CeO_2 content was corrected to the chemically-determined total (La, Pr, Nd, Sm etc.)$_2O_3+CeO_2$; the individual sesquioxide amounts, percentages and ratios were then calculated from this. The data are shown in Table 3.

Cerium is probably present in the cerous state in both the cerite and the allanite.[5] Account is to be taken of the fact, however, that cerous oxalate is oxidized to ceric oxide upon ignition in air and is weighed as such in quantitative determinations even when in admixture with typically trivalent rare earths.

INDIVIDUAL RARE EARTH RATIOS

Goldschmidt and Thomassen[6] in their classical study have subdivided rare earth minerals according to their average content of the individual rare earths as determined by x-ray spectrography. Both cerite and allanite (as well as bastnäsite, toernebohmite, eudialyte, eucolite, freyalite, melanocerite, mosandrite and tritomite) fall into their Class B, Subclass I, Type b. This class is that of minerals containing a selective group, rather than a complete representation, of the earths; in this subclass there is an outstanding content of cerium-group elements. The type is that of minerals with a high content of the elements La through Nd, and with only weak representation of Sm and Gd. Orthite (allanite) has lent its name to the type. This stands in contrast to the Monazite Type (a) which is similar but has high representation of La through Sm with still important amounts of Gd. There follows a comparison of our values with the Goldschmidt-Thomassen averages, representing the relative numbers of atoms, for this subclass. Shown also are ratios calculated from averaged arc spectrum data of McCarty[7] for 10 monazites as well as those calculated from other similar analyses reported by B. S. Hopkins et al.[8]

---

[5] Goldschmidt, V. M., Elemente und Minerale pegmatitischer Gestein: *Nachr. Ges. Wiss. Göttingen*, **1930**, *Math.-physik. Klasse, Fachgruppen IV Nr.* **4,** 370–378, has indicated that cerium is present in the ceric state in certain minerals of the alkaline nepheline-syenite pegmatites.

[6] Goldschmidt, V. M., and Thomassen, L., Röntgenspektrographische Untersuchungen über die Verteilung der seltenen Erdmetalle in Mineralen: *Videnskapsselskapets-Skrifter, I, Matemat. natur. Klasse, Kristiania*, No. 5 (**1924**).

[7] McCarty, C. N., Quantitative estimation of some of the rare earth ores by means of their arc spectra. *Doctorate Thesis, Univ. Illinois* (**1935**).

[8] McCarty, C. N., Scribner, L. R., and Lorenz, Margaret with Hopkins, B. S., Quantitative estimation of the rare earths by means of their arc spectra: *Ind. Eng. Chem., Anal. Edn.*, **10,** 184–187 (1938).

	57 La	58 Ce	59 Pr	60 Nd	61	62 Sm	63 Eu	64 Gd	65 Tb	66 Dy	67 Ho	68 Er	69 Tm	70 Yb	71 Lu
Colorado Cerite	24	47	ca.1	29	—	7	tr.	tr.	tr?	abs	tr.	abs	abs	abs	tr.
Colorado Allanite	35	32	≪1	35	—	6	abs	abs	abs	abs	abs	abs	abs	abs	abs
G. & T. Class B, Subclass I	12	50	8	24	0	7	0	4	0	ca. 2	—	—	-	—	—
10 Monazites[7]	19	45	9	25	—	3	—	6	–	—	—	–	—	—	—
1 Cerite[8]	15	not det.	not det.	30	—	6	—	2	—	1	—	—	—	1	—
1 Allanite, 1 Orthite[8]	not det.	not det.	not det.	24	—	7	—	4	—	3	—	—	—	2	—

In general the ratios reported at this time fit well into the average of the monazite and orthite types of Goldschmidt and Thomassen. While the latter did not report separate averages for the two types, and while the Illinois workers did not in some cases determine certain of the elements, some hypotheses may be put forward upon the above data. Thus it may be supposed that the Pr content of the subclass average is mainly due to a higher content of this element in monazite (and its associate, fluocerite or tysonite) than in cerite and orthite and their associates in the other type. Similarly, but on less conclusive evidence, one could assume the La content to be due to a greater extent to the allanite than to the monazite.

OCCURRENCE AND ORIGIN OF BABINGTONITE AND OTHER MINERALS FROM QUABBIN AQUEDUCT, MASSACHUSETTS

B. M. Shaub, *Smith College, Northampton, Massachusetts.*

Abstract

The suite of minerals from shaft 10 of the Quabbin Aqueduct is of more than usual interest, owing not only to the number of species that are present in the small veins and to the excellence of the minute crystals, but also to the presence of babingtonite at another locality in Massachusetts which gives the state 10 of the 14 known occurrences.

The question of origin is also one of special interest for the associated minerals, which with the exception of the feldspars and possibly the amphibole and mineral *X*, are characteristic of the mineral associations found in veins of the Connecticut Valley diabase of Massachusetts. As similar associations are not the usual products of residual solutions of acid magmas, the writer believes the solutions to have been derived, in their major portions at least, from very late fractions of a basic (gabbroic) magma.

The Quabbin Aqueduct, approximately 13 by 15 feet in cross-section, was driven between a point, shaft 1, on the Quinapoxet River near its entrance into Wachusett Reservoir, which is nine miles north of Worcester, and Quabbin Lake, a distance of 24 miles almost directly west. The tunnel is located at a depth of approximately one hundred to five hundred feet below the surface and transects the various schists, gneisses and igneous rocks at angles close to 90° to their strike. The excavations along the tunnel were conducted from a series of vertical shafts numbered from east to west. Shaft 10, from which the minerals were obtained, is located along Moose Brook at a point $2\frac{4}{5}$ miles N 44° E from Hardwick, Massachusetts.

The formation to the west of shaft 10 to shaft 11 consists entirely of Hardwick granite. This material is described by Emerson (1, p. 238) as being:

> . . . almost everywhere a black granite gneiss but in several small central areas what seems clearly to be a deep-seated core is exposed. . . . It is low in quartz and rather feldspathic, containing generally orthoclase, a little plagioclase, much biotite, much magnetite, hypersthene, zircon and allanite but no graphite or fibrolite.

To the east of shaft 10 the tunnel penetrates approximately 1600 feet of Hardwick granite, 2625 feet of Brimfield-Ware schist, 1225 feet of Coys Hill granite and then remains in Brimfield-Ware schist to shaft 9 for an additional distance of 9650 feet (2, Figs. 8D, 8E, 8F).

Emerson (1, p. 68) describes the Brimfield-Ware schist as:

> . . . the most marked and most widely distributed of the metamorphic formations assigned to the Carboniferous. The rock is a uniform coarse red-brown muscovite schist containing much biotite, fibrolite, and graphite and so much pyrite that it is wholly rusted in many of the deepest openings.

Regarding the Coys Hill granite, Emerson (1, p. 240) says:

> It is a regularly sheeted very coarse porphyritic microcline granite gneiss, in which the flat carlsbad twins are generally 2 to 4 inches square and three-fourths of an inch thick, and many of them are so closely set that there is little space for the coarse dark biotite-garnet ground mass, which winds in and out among them. These crystals have generally a granulated border from incipient crushing, which increases in thickness at the expense of the central crystal and is drawn out in the planes of the banding so that they form eye-like spots and finally complete crushing produces a medium-grained granite.

Diabase Dikes

At a point 4800 feet east of shaft 9 a diabase dike, 175 feet wide, was penetrated by the tunnel excavation. This is the only reference to basic intrusives (2) across the west end of the tunnel location.

As the fragments of the mineral-bearing veins occurred on the surface of the large dump after the excavating work had ceased, and after a part of the dump material had been crushed for the concrete mixture for the tunnel lining, it is somewhat uncertain as to the exact position of their original occurrence. It is reasonable, however, to believe that they originated about midway between shafts 9 and 10, or 10 and 11. The former location being in the Brimfield-Ware schist while the latter is in the Hardwick granite. As the veins occur in a pinkish granite, one may, therefore, assume that the point of occurrence is in the Hardwick granite about 1¼ to 1½ miles west of shaft 10.

Description of the Veins and the Granite Wall Rock

The majority of the veins are very small, usually less than ¾ inch across. One or two fragments of a vein-breccia less than 2 inches across were found. Unless the veins are very small (⅛ to ¼ inch) they are seldom completely filled but contain numerous cavities lined with minute crystals, often of superb quality.

A megascopic examination shows that the wall rock is composed, in general, of an equi-granular medium grained granite which consists of both pink and light colored feldspar which reach a maximum size of ¾ inch. Quartz occurs as light-grayish to white colored grains. The dark constituents consist chiefly of chlorite, magnetite and sphene. The chlorite represents altered biotite which is an important mineral of the Hardwick granite and is the main contributor to the "black" color of Emerson's description. Near the veins some epidote occurs as grains while at times it completely fills very small fractures which traverse the granite. In some specimens the chlorite becomes an abundant constituent and the rock becomes rather dark in appearance. In such specimens the feldspar is usually light-colored and the grain of the rock becomes finer. The chlorite and the other constituents are usually more or less banded and give the rock a gneissoid appearance. In addition, the following minerals are readily distinguished in hand specimens but do not always occur in thin sections: magnetite is probably the most abundant of these and is associated with the chlorite; sphene is rather conspicuous in a few specimens and common in most. Some specimens contain a number of allanite grains which stain the adjoining minerals, while a few grains of hornblende and an opaque black non-magnetic mineral were also observed.

A microscopic study shows that the three most abundant constituents are plagioclase, potash feldspars and quartz which produce an allotriomorphic medium-grained texture. The plagioclase is strongly altered to a very fine grained sericite. In some grains a rather fresh core of the plagioclase remains. The potash feldspars, orthoclase and microcline, are unaltered. The quartz contains many dust-like inclusions often in poorly defined bands; it also may show numerous incipient fractures arranged en echelon. The feldspars and quartz contain acicular crystals which are probably apatite. The biotite has been completely altered to chlorite. It occurs chiefly around the grains of the feldspar and quartz and usually in streaks. Whether the alteration is due to the vein solutions or to other more widespread phenomena could not be readily determined and was not investigated. Associated with the chlorite, which is strongly pleochroic from a brownish-yellowish green to deep emerald green, are small rounded grains of apatite. A few grains of zircon are present and these produce pleochroic halos in the chlorite.

The field geologists for the Water Commission (2) have recorded, in considerable detail, data concerning the character and structure of the rocks traversed by the tunnel. This information has been made available in the form of a descriptive elevation along the north wall together with a floor plan of the tunnel. From the section between shafts 9 and 10, and 10 and 11 one finds that numerous small pegmatites of various textures appear in all the formations and these pegmatitic phases vary in size from stringers and lenses to dikes more than five feet in thickness. The dip of the foliation is at a low angle of 10 to 25 degrees to the west.

The writer was unable to find any mention in this data of the occurrence of mineral veins of the type described here, which may be due to their small dimensions and while underground would be obscured by mud and rock dust. On the dump, after a rain, they would, however, readily attract the attention of mineral collectors.

Paragenesis of the Vein Minerals

The first increment of material deposited on the wall rock frequently consisted of additions to the quartz and feldspar already a part of the granite. These additions were not abundant and consisted chiefly of developing crystal faces, on earlier grains, often in parallel growth. Only rarely did these minerals continue to grow inward toward the center of the vein for any appreciable distance. Occasionally there are splendid crystals of albite which are only lightly attached to the walls so that they can be removed.

The first substantial deposition everywhere in the fractures consists of epidote which varies from a light yellowish-green to dark greenish-black. Scattered crystals of fluorite rest upon the epidote as well as upon the original wall-rock minerals in which instance they are often partly, and at times completely, covered with epidote. The fluorite is not abundant enough to completely cover the epidote over any appreciable area. Babingtonite frequently completely covers large areas of epidote and the scattered crystals of fluorite as well. Following the babingtonite in order of deposition are calcite and selenite, which are abundant enough to cover the preceding species; apophyllite sometimes completely covers babingtonite. Selenite is always the last mineral to be deposited. It frequently is present only as solution remnants scattered over large areas which indicates that it was originally much more abundant. Calcite likewise has been removed to a considerable extent by solution, and where these minerals do not appear in the veins it is not at all safe to assume that they were not present. One would probably be safer in assuming that both selenite and calcite were originally present in most of the veins unless the veins are small and completely filled by the earlier minerals.

The parts of the veins where deposition has been light one may find several of the earlier minerals attached to the walls singly or in small

TABLE 1. PARAGENESIS OF THE VEIN MINERALS

Wall Rock Minerals	Vein Minerals						
1	2	3	4	5	6	7	8
Quartz	*Albite*[a]	*Epidote*	*Fluorite*	*Babingtonite*	*Apophyllite*	*Calcite*	*Selenite*
Albite	Adularia	Fluorite	(blue)	Mineral X*	Heulandite		
Chlorite	Quartz	(colorless		Thomsonite*	Stilbite		
(of the		to amethyst)	Amphibole				
wall rock)			(fibrous)				
		Prehnite*					
Allanite			Galena*				
Magnetite			Sphalerite*				
Orthoclase			Pyrite*				
Sphene			Chlorite*				
Hornblende							
Microcline							

[a] The minerals in italics are the most abundant and persistent in their relationship to one another.

* In the specimens collected, these species were not covered by later minerals and hence may properly come under a later group, if the sequence were complete in all specimens.

groups without supporting later minerals. One may readily give a more inclusive or composite paragenetic picture and introduce the rarer species in the sequence as shown in Table 1.

With the exception of fluorite, the minerals in columns 4, 5, 6, 7 and 8 are sometimes absent. Minerals in columns 5, 6, 7 and 8 may be present singly or in combinations, except that calcite was not seen in association with the zeolites in such a manner that its sequence with respect to these minerals could be certain. However, rhombic cavities of presumably mineral X in calcite occur in one specimen which would place it earlier than calcite, and as the zeolites are not directly associated with calcite they too may be earlier in the general sequence as indicated. Calcite may belong in column 6 but its presence there could not be confirmed.

Origin of the Minerals

The origin of the minerals from shaft 10, except for adularia and albite, which are very closely associated with the minerals of the granite wall rock, is probably best determined by considering the probable origin of the solutions from which babingtonite in other occurrences crystallized. From thirteen (3, p. 302) out of the fourteen[1] authentic occurrences of babingtonite, seven are associated directly with veins in or at the contact of diabase, two occur with pegmatite granite, two with veins in gneiss and one each in granodiorite and diorite. Even the occurrence of babingtonite in pegmatite granite and in veins in gneiss does not exclude the possibility that the mineral solutions in these instances may have been mixed and that the essential constituents which were responsible for the formation of the babingtonite were derived from magma fractions, or segregations, of a far more basic character than the enclosing rock. *In each of the fourteen occurrences the mineral calcite is present and it may be the real marker in determining the origin of the solutions* which, in all cases, are undoubtedly the end product of the crystallization of some magma, or they may possibly have been produced during severe metamorphism as an end product of recrystallization during which process the water of crystallization of earlier minerals has been expelled together with some of the more soluble materials present. The end products of crystallization of acid magmas result almost universally in producing pegmatites, pegmatitic phases in the solidified parts of the magmas, or as mineral veins usually of an acid character and *exceptionally free from babingtonite.* The first two types of deposits unless contaminated from the enclosing rocks, or from other solutions, are comparatively free from calcite instead of this mineral being always or even frequently present. While calcite is somewhat more abundant in the mineral veins derived from acid magma solutions than in the pegmatites, nevertheless, it is not a mineral that is *always* present, even in small amounts. As the magmas become more basic, carbonate becomes more abundant in the late fractions and in the residual solutions. Veins formed from solutions from basic magmas usually contain calcite as one of the minerals. Wagner (5, p. 198) and Daly (6) describe carbonate dikes associated with the peridotite of the Premier Diamond Mine, Transvaal, South Africa. Small carbonate dikes up to two inches across occur in the Holyoke diabase[2] at the Amherst Notch Quarry where they represent very late fractions of the gabbroic magma.

---

[1] The fourteenth and as yet undescribed occurrence is in veins in the Holyoke diabase at the Amherst "Notch Quarry" about midway between Amherst and South Hadley, Massachusetts.

The nearest recorded diabase dike along the tunnel is nearly a mile east of shaft 9 and at least two to three miles from the nearest possible occurrence of the minerals, and in addition the schistosity of the formations dips at a low angle of 15 to 20 degrees to the west from the dike and toward the location of the mineral veins. Hence, it is hardly possible that the magma of this dike could have supplied the necessary solutions.

The most important data concerning the occurrence of babingtonite is that at least half of the occurrences of the mineral have been certainly derived from late diabase or gabbro solutions; and some of the other occurrences are closely associated with granodiorite, and diorite, rocks which are near relatives of gabbro. It is apparently important that one always finds calcite associated with babingtonite. With these pertinent facts bearing on the origin of babingtonite in other deposits, one may at least consider three possible sources for the mineral solutions that produced the minerals obtained from shaft 10.

For the first, one may consider the solutions as originating from a gabbro, or closely related magma, which crystallized in some unknown position not too remote from the occurrence of the mineral veins. Fracturing and brecciation of the granite about the intruded gabbroic magma provided fissures for the passage of hydrothermal fluids from the crystallizing magma, and also provided many voids for the development of the superb crystals that they now contain. It is known that a few isolated occurrences of diabase and other basic rocks occur to the east of the Connecticut Valley (1, p. 272) and many others may occur at unknown places within the rocks along the line of the tunnel.

As an alternative theory one may prefer to have the mineral-bearing solutions originate as late fractions of some basic differentiate of the granite, or a portion of the granite rendered initially basic by the assimilation of basic sediments or other earlier basic rocks.

---

[2] The fine-grained carbonate dikes and the coarse-grained phases of the Holyoke diabase at the Amherst Notch Quarry are being studied in detail.

One may also consider as a third possibility a theory which would account for the hydrothermal solutions as originating from (*a*) the crystallization of the normal granite, or (*b*) from the more basic parts which are quite rich in the black minerals biotite and magnetite; and (*c*) from the pegmatites associated with the granite or the pegmatitic phases of the granite.

If the solutions had originated according to the second or third conditions it would appear to the writer that babingtonite and the associated minerals should be of much more frequent occurrence in the Hardwick granite. Due to the lack of this more frequent occurrence, or the lack of knowledge concerning such occurrences, the writer tentatively considers the hydrothermal solutions to have originated from the crystallization of some gabbroic, or closely related magma, not too distant from the mineral veins and that the dynamic disturbances associated with the intrusion provided the necessary fracture system to convey the solutions and also provided spaces for the deposition of the minerals.

Brief Description of the Vein Minerals

Owing to the many splendid small crystals that occur among the species described below, a more detailed description of the morphology of many of them will follow at a later date. The following description of the minerals is arranged alphabetically rather than according to their abundance.

Adularia. Adularia is not very abundant and occurs chiefly as reddish to colorless crystals attached to the walls. The faces are usually dull and the body of the crystals contain many inclusions. They vary in size up to 3 mm.

Albite. Many splendid crystals of albite occur next to the granite walls to which they are usually firmly attached. Their development is chiefly parallel and close to the wall rather than projecting into the cavities. Occasionally well-developed crystals extend sufficiently far into the cavities so that they can be removed. They are often water clear and have brilliant faces. Their size is usually less than 3 mm.

Amphibole. A white to light cream colored fibrous amphibole consisting of small "pads" of extremely fine filamentary particles matted together and resembling "mountain leather" in appearance occurs on several specimens. It has a mean index of about 1.65 and occurs overlying epidote or between epidote and calcite.

Apophyllite. The largest and most conspicuous of the well-formed crystals are apophyllite. They vary in size from minute microscopic ones to slightly over a centimeter across. The smaller ones sometimes approach equidimensional proportions and are water clear while the larger ones are tabular and of a milky white color. They are next in abundance to babingtonite and in one specimen a large part of the babingtonite is completely covered. The corners of most of the crystals are truncated by the bipyramids.

Babingtonite. This mineral is probably next to epidote in abundance and frequently occurs as a continuous covering over an earlier deposit of epidote, which often in turn completely covers the walls. The crystals of babingtonite are short prismatic and usually possess brilliant faces. The larger crystals are jet black in reflected light while the smaller ones are of a distinct reddish-brown color. The size of individual crystals varies from less than a hundredth of a millimeter to 1½ millimeters. Several masses of babingtonite up to a centimeter across were observed. These are probably composed of compact granular aggregates.

Calcite. Calcite is among the more abundant minerals, but seldom occurs in good crystals for those present are usually strongly etched or even partly dissolved. Comparatively large masses occur covering epidote and small crystals are superimposed on babingtonite. One specimen of calcite contained rhombic cavities of an earlier mineral more soluble than calcite. The angles of the cavities are difficult to evaluate on account of their small size and the irregular enlargement by solution. These cavities are probably due to the mineral described below as mineral *X*.

Chlorite. As a distinct vein mineral chlorite is very rare. It was found in one specimen as clusters of extremely minute crystals covering adularia, quartz and lavender fluorite. It is strongly pleochroic in green and yellowish-green. Shreds of chlorite from the wall rock also project into the fissure for a short distance. The vein chlorite may represent material dissolved from the walls and redeposited in the fissure.

Epidote. Epidote is the most abundant mineral present and is readily recognized by its characteristic yellowish-green color in the smaller crystals and by the light greenish-yellow powder of the larger ones when crushed. The larger dense areas and the large crystals often appear dark green to black. They vary in size from small microscopic ones up to 2 mm. for those of more or less equidimensional proportions. In only two specimens did the habit vary in which instances the crystals formed small groups radiating from common centers. The epidote is often overlain by babingtonite, selenite, calcite and to a much less extent by fluorite. The equidimensional crystals are of a superb character for morphological studies which are now in progress.

Fluorite. The first deposition of fluorite occurred simultaneously with epidote and continued later, producing well-developed crystals superimposed on the epidote. Fluorite varies considerably in its habit. It is commonly present as octahedrons more or less rounded and in irregular masses varying from colorless to a deep lavender color. On some specimens the octahedrons are very sharply developed and have glistening faces. Occasionally the fluorite is of a deep blue color and the octahedrons are then modified by cubes and the trisoctahedral forms.

Galena-Anglesite. Two crystals of galena were found resting on albite, one was a well-developed unmodified octahedron. A white coating, which is soluble in nitric acid without effervescence, surrounded the crystals. It is probably the lead sulphate, anglesite.

Heulandite. This is one of the less abundant species. It occurs sparingly on a few specimens. In one instance it consists of a group of fine transparent crystals about ½ to 1 mm. in size.

Limonite. The veins are almost free from the effects of oxidation and only a few "rusty" spots occur where minute crystals of pyrite have altered to limonite.

Prehnite. Prehnite was observed on only one specimen which consisted of brecciated granite loosely cemented by the vein minerals. Numerous open spaces remained for the development of many fine crystals of epidote, fluorite and albite. With these the prehnite occurs as one of the earlier to crystallize. It consists of the characteristic bunch-like or spherical aggregates, and is of a slight bluish-green color.

Pyrite. Sulphides are very rare in this mineral occurrence. Only a few small crystals of pyrite were observed usually unaltered and consisting of cubes modified by pyritohedrons.

Quartz. As a strictly vein mineral, quartz must be considered to be among the less plentiful species. Although the wall rock contains an abundance of quartz, the typical terminated quartz crystal projecting into the fissure is indeed rare. It appears that the quartz grains in the wall rock started a renewed growth by developing crystal faces in parallel position and remaining close to the vein fractures in the same manner as albite.

Selenite. At one period, selenite was much more abundant than at present as much of it has been removed in solution, for the material now present is clearly the remnants of solution processes. All crystal forms, if they ever existed, have been completely removed. The material is white to transparent in color and forms a protecting cover for epidote, fluorite, stilbite, babingtonite apophyllite and mineral *X*. Where the selenite has been dissolved from these minerals they remain as splendid brilliant crystals. The underlying minerals may be readily obtained on account of the softness and easy cleavages of selenite, together with the lack of adhesion of the selenite to the earlier minerals.

Sphalerite. A single greenish crystal of sphalerite was found on epidote. Its very high index, dodecahedral cleavage and optical isotropism easily distinguish it from other minerals.

Stilbite. A few specimens contained small groups of isolated stilbite crystals of a lath-like habit. Stilbite is contemporaneous with apophyllite and both are covered by selenite.

Thomsonite. A few nearly equidimensional crystals of thomsonite having a very faint pink color occur with epidote and mineral *X*. They do not have good crystal faces and were undoubtedly covered by selenite, the solution remnants of which adjoin the crystals.

Mineral X. The identity of this white, monoclinic mineral which occurs in very small amounts is in doubt. Its mean index of refraction is close to 1.507, it has a large optic angle and an extinction angle of nearly 40 degrees and a low birefringence. A few fair to good, but very small, crystals occur in and around selenite. It is hoped that sufficient material will be found to obtain the necessary information for its identification.

REFERENCES

1. Emerson, B. K., Geology of Massachusetts and Rhode Island: *U. S. G. S. Bull.*, **597** (1917).
2. Annual report of the Metropolitan District water supply commission for the year ending November 30, 1935: *Public Document No. 147 of the Commonwealth of Massachusetts.*
3. Palache, Charles, and Gonyer, F. A., On babingtonite: *Am. Mineral.*, **17,** 295–303 (1932).
4. Palache, Charles, Babingtonite and epidote from Westfield, Massachusetts: *Am. Mineral.*, **21,** 652–655 (1936).
5. Wagner, Percy Albert, The diamond fields of southern Africa: *The Transvaal Leader*, Johannesburg (**1914**).
6. Daly, Reginald A., Carbonate dykes of the Premier diamond mine, Transvaal: *Jour. Geol.*, **33,** 659–684 (1925).

NOTES AND NEWS

PYROSTILPNITE FROM RANDSBURG, CALIFORNIA

JOSEPH MURDOCH, *University of California at Los Angeles.*

The rare mineral pyrostilpnite (Ag_3SbS_3) has been found recently in small amount among the silver minerals of the California Rand mine, in the Randsburg district, California. So far as the writer is aware, this is only the second known occurrence of this mineral in North America. The original discovery was of a single crystal associated with miargyrite in the silver ores of the De Lamar mining district, Idaho.[1] It has been reported from Chañarcillo, Chile, by Streng,[2] but according to Schrauf,[3] this mineral is probably rittingerite, as the angles correspond almost exactly with the latter. Streng[4] agrees that it may be rittingerite, but considers the whole question of these minerals as still unsolved.

The Randsburg material was found mainly on one small hand specimen, which according to the mine manager probably came from near the 700′ level, although this is not positive. Another specimen, from the 850′ level, collected by the writer, carries a very few minute crystals of the mineral. The richer specimen is composed largely of a vein of massive miargyrite, which presents a leached and vuggy appearance. The vugs are lined with a botryoidal coating of cervantite ranging from colorless to clear yellow and opaque white. There is also a considerable amount of this mineral here as a coating of microscopic crystalline grains, usually surmounting the amorphous crust. Partly on this coating, and partly enveloped by it, occur sparsely scattered grains and crystals of pyrostilpnite, and also a few crystals of pyrargyrite.

The pyrostilpnite was identified by its physical properties, and by microchemical tests for silver, antimony and sulphur. The presence of silver and antimony were confirmed by spectroscopic analysis. The extremely small amount of material available did not permit quantitative determinations. The mineral occurs both as single, flattened crystals and as sub-parallel or radiating clusters of blade or needle-like crystals. Even those crystals which seem to be single individuals are frequently modified by minute flake-like crystals in essentially parallel position.

---

[1] Lindgren, Waldemar, The gold and silver veins of Silver City, De Lamar, and other mining districts in Idaho: *U.S.G.S., 20th Ann. Rept.*, pt. 3, 169 (**1900**) [a note by Penfield].

[2] Streng, A., Mineralogische Mittheilungen über die Erze von Chañarcillo in Nordchile: *Neues Jahrb. Mineral., etc.*, 918 (**1878**).

[3] Schrauf, A., Feuerblende, Rittingerit von Chañarcillo: *Neues Jahrb. Mineral., etc.*, 144 (**1879**).

[4] Streng, A., Feuerblende und Rittingerit: *Neues Jahrb. Mineral., etc.*, 547 (**1879**).

The crystals are all very small, ranging in length from 0.5 to 0.1 mm. In shape they are usually elongated and lath-like, with the smaller dimensions from one-fourth to one-tenth of the length. Less commonly the crystals are nearly equidimensional prisms, or hair-like forms. In general, the color is the normal orange red, with strongly pearly luster on the broad side pinacoids, but some are partially blackened, at least on their surface, by some sort of alteration. Many of the crystals are fairly well terminated.

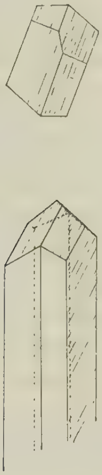

Fig. 1

Measurements on the goniometer are not particularly satisfactory, because of the presence of numerous striations on the faces, shown in the drawing of a typical crystal (Fig. 1), but in general they correspond reasonably well with those of Luedecke.[5] Microscopic examination of these crystals shows, as is apparently the case with all crystals which have been studied, that they are complexly twinned internally. Since this is the case, the interpretation of forms on a monoclinic basis is rendered very uncertain. Furthermore, optical study has suggested[6] that the mineral may well possess triclinic symmetry. In view of these complications, it has seemed desirable to withhold, for the present, the crystallographic data obtained from this material, in the hope that later work may solve the problem.

[5] Luedecke, Otto, Ueber Feuerblende von St. Andreasberg: *Zeits. Krist., Min., etc.*, **6**, 570 (1882).

[6] Dr. Harry Berman, private communication.

The spectroscopic analysis was made possible by a grant from the Research Fund of the University of California.

MOLYBDENITE AT MAGNET COVE, ARKANSAS

V. G. Sleight, *University of Arkansas, Fayetteville, Arkansas.*

Magnet Cove, Arkansas, has long been famous for the wide variety of its mineral specimens and the writer wishes to add molybdenite to the list. As groups of people continue to visit the area and gradually wander farther from the more frequented stops, the list of minerals reported from that region should grow to some extent, but Williams' (1891) report will continue to be the authority.

On the annual spring field trip from the University of Arkansas in 1940, molybdenite was found near the north rim of the Cove on the northwest bank of Cove Creek in the southwest quarter, of the northeast quarter, of section 17, T. 3 S., R. 17 W., across the road from a yellow brick bungalow. The molybdenite is disseminated throughout two or three cubic feet of gray, siliceous material that is probably another occurrence of geyserite which is found at other localities within the Cove. Masses (up to four inches in diameter) of granular and crystalline pyrite are associated with the silica and small (1/32 to 1/8 inch) crystals of apatite occupy cavities. In one or two places the molybdenite is abundant enough to give a blue cast to the rock. Another specimen obtained shows a coating of molybdenite covering striated pyrite crystals. This coating is very thin and is easily removed leaving the crystal faces of the pyrite unchanged. It apparently does not penetrate the pyrite crystals except in preexisting cracks.

The bluish gray color of the molybdenite itself, its streak on paper, and the greenish color of the streak on glazed porcelain are characteristic. A chemical check was made by using the thiocyanate test.

In visiting Magnet Cove the writer has found it convenient to have a list of minerals occurring there, and the accompanying list has been compiled from the reports of Williams (1891), Landes (1931), and Landes, Parks, and Scheid (1932). Crystal fragments and an occasional good crystal of the minerals marked with an asterisk are abundant on the roadside bluffs at Cove Creek bridge, the Magnet cemetery, and at the Titanium Corporation strip pits.

Alphabetically Arranged List of Magnet Cove Minerals

- actinolite
- aegerite (acmite)*
- albite
- allophane
- aluminite
- ankerite
- apatite
- aragonite
- astrophyllite
- augite
- biotite*
- braunite
- brookite (arkansite)*
- brucite
- calcite*
- cancrinite
- catapleiite
- cordierite (iolite)
- eucolite
- eudyalite
- fluorite
- garnet
    - almandite
    - andradite (melanite)
    - grossularite
- graphite
- hematite
- hornblende
- hydrotitanite
- hypersthene
- ilmenite
- limonite
- magnetite*
- manganopectolite
- microcline
- molybdenite
- monticellite
- natrolite
- nepheline
- octahedrite
- oligoclase (sunstone)
- olivine
- opal (geyserite)*
- orthoclase
- perovskite
- phlogopite
- plagioclase
- pseudoleucite
- pyrite*
- quartz
    - aventurine
    - milky
    - novaculite
    - rock crystal*
- smoky
- rutile*
- schorlomite
- sodalite
- sphene*
- thomsonite (ozarkite)
- variscite
- vermiculites*
- vesuvianite (idocrase)
- wollastonite
- xanthophyllite

Bibliography

Landes, K. K., A paragenetic classification of the Magnet Cove minerals: *Am. Mineral.*, **16,** 313–326 (1931).

———, Parks, Bryon, and Scheid, V. E., Magnetic Cove, Arkansas, *International Geological Congress, 16th session, Guidebook* **2,** Excursion a-2, 104–112 (1932).

Williams, J. F., The igneous rocks of Arkansas: *Arkansas Geol.* Surv., *Annual Rept.* **1890,** vol. 2, 163–343 (1891).

A CHECK ON UNIT CELL CONSTANTS DERIVED FROM 1-LAYER-LINE WEISSENBERG PICTURES

C. W. Wolfe, *Harvard University, Cambridge, Mass.*

Buerger (*Am. Mineral.*, **22,** 416–435, 1937) has summarized the methods of obtaining all lattice constants from one crystal setting. A check on the constants which are derived from 1-layer-line Weissenberg pictures is here proposed, since these constants cannot be obtained so accurately, as a rule. The volume of the unit cell of a triclinic mineral may be computed from constants derived from rotation and 0-layer-line pictures, alone. The result is more accurate than that obtained when constants derived from the 1-layer-line picture are also used. Consequently, any considerable variation in the volumes obtained in these two ways indicates an error in the determination of the 1-layer-line constants. For example:

Rotation and 0-layer-line Weissenberg pictures about $c[001]$ give the values for a^*, b^*, γ^* and c_0, all of which may be accurately derived. Now:

$$a_0=\frac{\lambda}{a^*}\cdot\frac{1}{\sin\beta\sin\gamma^*}=\frac{d_{(100)}}{\sin\beta\sin\gamma^*};\quad b_0=\frac{\lambda}{b^*}\cdot\frac{1}{\sin\alpha\sin\gamma^*}=\frac{d_{(010)}}{\sin\alpha\sin\gamma^*}.$$

The volume is:

$$\begin{aligned}V_0&=a_0b_0c_0\sin\alpha\sin\beta\sin\gamma^*\\&=\frac{\lambda}{a^*\sin\beta\sin\gamma^*}\cdot\frac{\lambda}{b^*\sin\alpha\sin\gamma^*}\cdot c_0\sin\alpha\sin\beta\sin\gamma^*\\&=\frac{\lambda^2c_0}{a^*b^*\sin\gamma^*}=\frac{d_{(100)}\cdot d_{(010)}}{\sin\gamma^*}c_0\,.\end{aligned}$$

BOOK REVIEW

SEDIMENTARY PETROGRAPHY by Henry B. Milner. Third edition. XXIII+666 pages, 52 plates, 100 figures. Thomas Murby & Co., London; Nordeman Publishing Co., New York. 1940. Price $10.00.

Since the appearance of the second edition of this well-known text in 1929 great strides have been made in the study of sedimentary materials. This is particularly true of the present technique employed in investigating clays and soils. In order to present these modern procedures as well as outline the application of petrographic methods in certain industries, the author has found it necessary to materially revise and expand the earlier edition. The present third edition contains approximately 150 more pages and a change has likewise been made to a larger format (demy 8-vo instead of crown 8-vo).

Additional data are recorded on descriptive mineralogy while the portion devoted to laboratory technique has been expanded to six chapters covering mechanical analysis, *x*-ray, spectrum, fluorescence, and microchemical and microscopical methods employed in the solution of practical problems where sedimentary materials are involved. In the chapter on "Applied Sedimentary Petrology" interesting suggestions are given in the application of optical methods to problems relating to the asphalt industry, ceramics, highway construction, refractories, industrial maladies, and to building and glass technology.

The determinative tables of the former edition have been replaced by a series of appendices listing the essential physical and optical properties in order of increasing numerical values. The book can serve as a comprehensive treatise on the petrology of both consolidated and unconsolidated sediments and is indispensable to petrographers interested in this field, although the high price will no doubt restrict its sale.

W.F.H.

NEW MINERAL NAMES

Saamite

M. I. Volkova and B. V. Melentiev: *Comp. Rend.* (Doklady) *Acad. Sci., U. S. S. R.*. **25**, 120–122 (1939).

Name proposed for high strontium apatites from Poachvumchorr, Takhtarvumchorr and Aevesogchorr, Kola Peninsula, U. S. S. R. They differ from the other apatites of the region in their higher SrO content (6–11%, as opposed to 2–3%).

J. P. Marble

Titano-lovenite =(låvenite)

E. I. Kutukova: Titano-lovenite of the Lovozero tundras, *Trans. Inst. Geol. Sci., Acad. Sci. U. S. S. R., Fasc.* **31**, *Mineral.-Geochem. Ser.* (No. 6) 23–29, (**1940**), 2 fig. [Russian, with English summary.]

Essentially låvenite (Brøgger, 1885), with TiO_2 11.30% in place of about 2.00% in the original species. Physical and chemical properties as for låvenite.

Optical Properties: Optically—; $n_g=1.760$, $n_m=1.746$, $n_p=1.720$; $2V=73–74°$. Pleochroism distinct: n_g=orange-yellow, n_m=weakly greenish-yellow, n_p=pale yellow with a greenish tint.

Occurrence: Found as xenomorphic grains up to 0.5 mm. diameter in aplite stringers and hornblende syenite, in the central part of the Lovozero alkaline massif, on the Koklukhtiyai River, Kola Peninsula, U. S. S. R.

J.P.M.

Jarošite

Jaroslav Kokta, Einigen sulphaten von Smolnik in Slovakia: *Sbornik Kl. Prir. Brne*, **19**, 75–79 (1937), through *Min. Abs.*, **7**, 316 (1939).

Name: For Zdeněk Jaroš, keeper of minerals in the museum at Brno. (Pronounced jaroschite, yarroshite).

Chemical Properties: A magnesian melanterite, $(Fe, Mg)SO_4 \cdot 7H_2O$. Analysis: SO_3 30.13, FeO 17.10, CuO 0.04, MgO 5.55, H_2O 47.30; sum 100.12.

Physical Properties: Sp. gr. = 1.818. Optically negative, $n = 1.471 - 1.478$ on (001).

Michael Fleischer

Cuprojarosite

Jaroslav Kokta, *op. cit.*

Chemical Properties: A magnesian cuprian melanterite. Analysis: SO_3 29.93, FeO 15.18, CuO 4.40, MgO 4.29, MnO tr., H_2O 46.50; sum 100.30.

Physical Properties: Sp. gr. = 1.868. Optically positive, mean **n** = 1.472.

M. F.

Kirovite

G. N. Vertushkov, Kirovite and cuprokirovite—new minerals from the pyrite conflagrations of the Urals: *Bull. Acad. Sci. URSS, Sér. Geol.*, **1939**, pp. 109–115; through *Min. Abs.*, **7**, 418 (1940).

Chemical Properties: A magnesian melanterite. Analysis: SO_3 30.51, FeO 12.75, MgO 7.45, ZnO 0.50, CuO 0.30, MnO 0.18, Al_2O_3 1.42, CaO tr., H_2O 46.68; sum 99.79.

Crystallographic Properties: Monoclinic, pseudo-octahedral, $a:b:c = 1.1746:1:1.5323$, $\beta = 75°38'$. Cleavages (110) perfect, (001) less perfect.

Physical Properties: Sp. gr. = 1.76, H. = $2\frac{1}{2}$. Optic axial plane (010), $\gamma:c = 12°$, $\alpha = 1.467$, $\gamma = 1.476$, 2V large, positive.

Occurrence: Abundant as large yellowish-green stalactites and stalagmites on walls and mine timbers of the Kalata mine, Kirovgrad, where fires have enriched mine waters in sulfates.

M. F.

Cuprokirovite

G. N. Vertushkov, *op. cit.*

Chemical Properties: A magnesian cuprian melanterite. Analysis: SO_3 30.11, FeO 18.48, MgO 3.36, ZnO 0.38, CuO 3.18, MnO 0.05, Al_2O_3 0.29, Fe_2O_3 0.22, H_2O 44.50, CaO tr.; sum 100.57.

Physical Properties: Monclinic. Pale blue. Sp. gr. = 1.81.

$\alpha = 1.469$, $\gamma = 1.478$.

Occurrence: Same as kirovite.

Discussion: The literature is burdened with four unnecessary names for varieties of melanterite. The name jarošite is particularly bad because it is so readily confused with jarosite.

M. F.